

UVM ScholarWorks

The Role Of N-Terminal Acidic Inserts On The Dynamics Of The Tau Protein.

Item Type	thesis;article
Authors	Redmond, Miranda
Download date	2026-06-16 09:03:23
Link to Item	https://hdl.handle.net/20.500.14849/4740

THE ROLE OF N-TERMINAL ACIDIC INSERTS ON THE DYNAMICS OF THE TAU
PROTEIN.

A Thesis Presented

by

Miranda Redmond

to

The Faculty of the Graduate College

of

The University of Vermont

In Partial Fulfillment of the Requirements
for the Degree of Master of Science
Specializing in Cellular, Molecular, and Biomedical Sciences

May, 2017

Defense Date: March 17, 2017
Thesis Examination Committee:

Christopher Berger, Ph.D., Advisor
Bryan Ballif, Ph.D., Chairperson
Jason Stumpff, Ph.D.
Kathy Trybus, Ph.D.
Dave Warshaw, Ph.D.

Cynthia J. Forehand, Ph.D., Dean of the Graduate College

ABSTRACT

Alzheimer's disease (AD), the most prevalent neurodegenerative disease, is characterized in part by disruptions in axonal transport. Axonal transport is a process by which motor proteins carry organelles and other cargo made in the neuronal cell body along microtubule tracks to distal regions of the axon. The microtubule-associated protein (MAP) Tau plays a crucial role in regulating axonal transport, and is implicated in the development of AD and other types of dementia collectively known as Tauopathies. Tau is a neuronal-specific MAP that has six isoforms alternatively spliced from a single gene. These isoforms differ by the presence of zero, one, or two N-terminal acidic inserts and three or four C-terminal microtubule binding repeats. Tau is also known to be an intrinsically disordered protein that undergoes a dynamic equilibrium between static and diffusive states on the microtubule surface. The dynamics of Tau are important in the regulation of motor protein mediated axonal transport in neurons. Isoform-specific differences in the dynamic behavior of Tau on the microtubule surface, however, are not yet fully understood. Diffusive Tau is thought to be stabilized by electrostatic interactions between its N- and C-termini while static Tau is proposed to be extended with its C-terminal repeats contacting the microtubule and the N-terminus projected away from the microtubule surface. Thus, the N-terminal inserts may help regulate Tau's dynamic behavior and function during axonal transport. In this study, the dynamics of two different isoforms of Tau, both with three-microtubule binding repeats but a different number of N-terminal acidic inserts, were assessed using single molecule imaging techniques and novel data analysis methods.

ACKNOWLEDGEMENTS

This research was conducted with Funding from the NIH to Dr. Christopher Berger (GM101066) and a CMB Graduate Teaching Fellowship. Thank you to the Cell, Molecular, and Biomedical Sciences Program for their support; particularly Jessica Deaette, Carrie Perkins, Erin Montgomery, Kristin van Luling, Matt Poynter, PhD, and Nicholas Heintz, PhD. Thank you to the Molecular Physiology Department. In particular thank you to Dave Warshaw, PhD, Julie Lovelette, and Margaret Corson. Thank you to the Warshaw Lab for the use of their equipment and expertise and to Guy Kennedy for his TIRF scope training and support. This work would not have been possible without the training by Lynn Chrin, Jamie Stern, and Greg Hoepflich, PhD. Thank you to them and other members of the Berger and Stumpff Labs for their support. The MATLAB codes were written by Rehan Ali, as well as the training on using and understanding the codes. Finally, thank you to Chris Berger, PhD for his support and guidance throughout this project and graduate school.

Thank you to the members of the thesis committee for their continued support and expertise, Jason Stumpff, PhD, Kathy Trybus, PhD, Dave Warshaw, PhD, and the committee chair Bryan Ballif, PhD.

TABLE OF CONTENTS

	Page
ACKNOWLEDGEMENTS.....	ii
LIST OF ABBREVIATIONS.....	vi
LIST OF FIGURES.....	vii
LITERATURE REVIEW.....	1
Overview.....	1
Alzheimer’s disease is a devastating type of neurodegeneration.....	1
Pathological Features of Alzheimer's disease.....	3
Tau is implicated in Alzheimer’s disease.....	5
Tau contains an N-terminal projection domain that contributes to its different proposed functions.....	6
The Tau protein has six isoforms with common regions between the molecules.....	8
Tau converts between diffusive and static states on the microtubule.....	8
Tau adopts some known features as it transitions into the disease state.....	9
Alzheimer’s disease is known to have disruptions in axonal transport.....	10
Motor proteins such as kinesin transport cargo along microtubules.....	12
Kinesin-1 motor proteins walk along microtubules decorated with proteins and modifiers.....	14
The longest and shortest isoforms of Tau can differentially modulate kinesin-1 active transport in the axon.....	15
Tau has additional roles in axonal transport.....	15
Tau does not have a known structure on the microtubule.....	16
N-terminal acidic inserts may have an effect on the dynamic equilibrium of Tau.....	18

Differences between the six isoforms of Tau needs to be better understood.....	19
Previous methods of data analysis may not have been sensitive enough to capture all events in single molecule assays.....	19
MATERIALS AND METHODS.....	21
Plasmid Purification and Protein Prep.....	21
Tau labeling with Alexa 488.....	23
Diffusion Assay: Tubulin Polymerization.....	24
Diffusion Assay: TIRF Assay.....	24
Diffusion Assay: Data Analysis.....	25
Data Analysis: MatLab.....	26
Data Analysis: Statistics.....	27
RESULTS.....	29
Characterization of the 3RS and 3RL isoforms.....	29
3RS and 3RL are found more often in the static state than the diffusive state.....	29
3RS and 3RL have longer static dwell times than diffusive dwell times.....	30
3R-Tau is more likely to switch from the diffusive state into the static state.....	30
3RS and 3RL Tau are diffusive with no directed motion.....	31
3RS and 3RL have much shorter dwell times than previously reported.....	31
DISCUSSION.....	32
3RS- and 3RL-Tau have similar dynamic equilibriums favoring the static state.....	32
The novel data analysis method was more sensitive and captured many more short events than previous methods.....	32
3R-Tau is more likely to switch from the diffusive state into the static state.....	33
3RS and 3RL-Tau have similar dynamic equilibriums.....	34

Tau is a purely diffusive molecule, with no directed motion or direction bias.....	35
FUTURE DIRECTIONS.....	36
Evaluating Isoform Specific Differences.....	36
Further work is needed to characterize 3R-Tau’s behavior on the microtubule...	36
Isoform Differences on Kinesin-1 motility and signaling.....	37
CONCLUSION.....	39
FIGURES.....	40
WORKS CITED.....	55

LIST OF ABBREVIATIONS

activities of daily living (ADL)

Alzheimer's disease (AD)

central nervous system (CNS)

gray matter (GM)

histone deacetylase 6 (HDAC6)

means squared displacements (MSD)

medial temporal lobe (MTL)

medial temporal lobe atrophy (MTA)

microtubule-associated proteins (MAPs)

microtubule-binding repeats (MTBRs)

mild cognitive impairment (MCI)

neurofibrillary tangles (NFTs)

paired helical filaments (PHFs)

peripheral nervous system (PNS)

post-translational modifications (PTMs)

proline-rich region (PRR)

white matter (WM)

LIST OF FIGURES

Figure	Page
Figure 1: Necrosis is found in different regions of the brain in AD.....	40
Figure 2: Neurons are a highly polarized cell in the brain.....	41
Figure 3: Tau has six isoforms alternatively spliced from the same gene on chromosome 17.....	42
Figure 4: Tau is involved in kinesin-1 inhibition, microtubule stabilization, and signaling pathways.....	43
Figure 5: A proposed model shows how Tau is a conformationally dynamic protein converting between a static and diffusive state on the microtubule.....	44
Figure 6: Kinesin-1 hydrolyzes ATP with each step it takes.....	45
Figure 7: Kinesin-1 is inhibited by Tau.....	46
Figure 8: Sample kymographs of Tau show molecules in different states.....	47
Figure 9: Characterization of the protein prep and labeling of the 3R-isoforms.....	48
Figure 10: A sliding window analysis was used to characterize Tau events.....	49
Figure 11: 3RS and 3RL favor the static state at a 2:1 ratio and have longer static dwell times than diffusive dwell times.....	50
Figure 12: 3RS and 3RL switch more often from the diffusive to static state.....	51
Figure 13: 3RS and 3RL favor the static state at a 2:1 ratio.....	52
Figure 14: 3RS and 3RL in the diffusive state have no directed motion.....	53
Figure 15: 3RS has much shorter dwell times in this data analysis than previous ones.....	54

LITERATURE REVIEW

Overview

This literature review will address from global to the molecular the role of the protein Tau in the developed adult brain. The work will begin with a look at the gross features of Alzheimer's disease (AD), some of the known pathological features of AD, and then look at proposed molecular causes. One of these proposed molecules involved in AD is the protein Tau. The literature review will therefore look at what is known about the structure and function of Tau and its known roles in the neurons. One of these is Tau's influence on axonal transport and how that process is disrupted in AD. The review will then introduce how Tau's role in axonal transport is related to its dynamics behavior on the microtubule surface. The current understanding is that Tau binds to microtubules in both diffusive and static state but little is currently known about differences in dynamic behavior among different isoforms of Tau. This study examines the differences in dynamics of two Tau isoforms, 3RS and 3RL. In addition, this research will look at previous work and limitations of the previous data analysis methods used. The current research will introduce a novel data analysis method designed to eliminate subjectivity and be more sensitive to short time-scale events. Overall, the literature review will look at the pathological features in AD to the physiological processes. This will highlight the need to better understand the Tau proteins function and its role in neurodegeneration.

Alzheimer's disease is a devastating type of neurodegeneration.

Alzheimer's disease (AD) is one of the most common types of dementia affecting approximately 5.4 million people in the United States¹, yet an estimated half of cases go undiagnosed². Since a decrease in cognitive function is normal with aging, distinguishing

the transition from normal cognitive decline to mild cognitive impairment (MCI) to AD must occur with coordination by the patient, caregivers, and health care providers. Patients are often seen in clinics or elsewhere where cognitive decline is a secondary or tertiary concern³. Health care providers must, therefore, recognize early symptoms of AD for close monitoring.

Although important to recognize, an early diagnosis does not necessarily correlate with a longer lifespan or quality of life in those affected. Lifespans and death rates from AD remain difficult to categorize since patients often have a primary cause of death other than AD. The cause of death may be directly or indirectly related to the person's cognitive decline and losses in activities of daily living (ADL). These include susceptibility to infection, depression, or muscle atrophy if a patient becomes bedridden. Estimates for 2016 predicted that over 700,000 people in the United States would die that year *with* AD¹. Reporting standards still may not be capturing all AD-related deaths, particularly if a case was not diagnosed ante-mortem.

The prevalence of AD has grown rapidly over the past hundred years since Dr. Alois Alzheimer first described the disease in 1906. This is partly an artificial increase as more education on the disease has led to more screens in at-risk patients. The numbers of deaths from the disease have therefore risen because of the increase in people in the United States diagnosed with AD. In addition, since studies have shown a greater risk of developing AD with increasing age⁴, the rates of AD will continue to increase as life expectancies increase. In the 2016 statistics for the United States, 44 percent of those with AD were aged 75 to 84, and 37 percent were 85 or older¹. The majority of people in the United States with AD are, therefore, above 75 years old due in part to longer life

expectancies and better diagnostics.

With these rising rates of AD, it is imperative to understand how the disease state differs from typical aging patterns. According to the 2013 APA guidelines, a patient can receive an AD diagnosis if their symptoms involve a loss of one of the following: coherent speech, spoken or written language comprehension, object identification, basic motor skills, abstract thinking, or multi-command tasks. The presence of these symptoms must be medically verified and occur along with a memory decline and, critically, disrupt capable daily living⁵. These guidelines will help standardize diagnosis of AD by health care providers but must be complemented with a better understanding of underlying molecular mechanisms, disease markers, and diagnostic tools.

Pathological Features of Alzheimer's disease

The APA guidelines are a useful but not complete criterion for an AD diagnosis. Medical imaging techniques have become more advanced, thereby increasing AD detection sensitivity. They are limited though because the disease is not isolated to a discrete part of the brain. Much is still not understood about the tissue atrophy seen in the brain in AD. Current research in the field has not come to a complete consensus about the sites of initial degeneration and whether the atrophy seen in different brain regions is connected or develops independently. What is known is that there are common patterns of atrophy in regions of the brain that include, with overlap; the limbic system, medial temporal lobe, frontal temporal lobe, and hippocampus (Figure 1).

One confirmed pathology is that the atrophy seen throughout the brain originates from massive cell death of neurons, the primary cell of the nervous system (Figure 2). These neurons are responsible for signaling, cognition, and motor coordination. Neurons

have several defining features including the cell body, known as the soma, with multiple projections radiating off of the soma. These projections are differentiated into dendrites and axons. The *dendrites* are smaller and more numerous projections that receive the signals. The signaling is then propagated through the longer extensions known as *axons*. Most axons extend several microns away from the soma although, in extreme cases, axons can extend up to one meter. The range of dendrite compositions, axons, and their lengths correlates with the diversity of functions required by neurons found in both the central nervous system (CNS) and peripheral nervous system (PNS).

Within these regions there are gray matter (GM) and white matter (WM) atrophies. The GM atrophies are from degeneration of the *cell bodies* or *soma* of central nervous system (CNS) neurons, while WM atrophies are degeneration of the CNS *axons*. Both atrophies are present in AD but it is not clear if the observed degenerations are connected, dependent, or entirely independent from each other⁶. Different studies have contradictory results with finding ranging from AD as a GM disease with WM atrophy a secondary effect to other studies showing no long-term connection³. Another hypothesis suggests that WM degeneration precedes GM atrophy⁷. The difference may be region specific as some correlation of GM and WM atrophy is seen in the hippocampus⁶ but there is little connection in the entorhinal cortex⁸. This field needs more study to understand the interplay between different brain regions and specific patterns of neurodegeneration present.

In addition to atrophies in different regions of the brain occurring in afflicted individuals, AD patients exhibit different levels of global neurodegeneration and reduction in brain volumes. The necrosis in AD is not entirely generalizable but some

common features have been observed. Globally there is an average 15% reduction of hippocampal volume per year in patients with AD compared to a 1.5% reduction in age-correlated cognitively-normal individuals⁹. In addition, 80-90% of AD patients have medial temporal lobe atrophy (MTA) on both the hippocampus and entorhinal cortex (Figure 1)².

While research in Alzheimer's disease has increased exponentially since the time of Dr. Alois Alzheimer and Dr. Emil Kraepelin in 1906, there is still relatively little understood about this devastating disease. The underlying causes of the neurodegeneration are multidimensional and it is not clear how changes on the molecular level translate into the observed neurodegeneration. Within neurons several molecular factors are *implicated* in AD, but not entirely understood. The transition from healthy neurons to diseased ones is unclear but understanding the molecular markers is important for early detection and identifying therapeutic targets.

Tau is implicated in Alzheimer's disease.

The gross atrophies seen in the brain have a biochemical commonality as two macromolecules have been shown to aggregate in neurons of the medial temporal lobe (MTL). These molecules are thought to disrupt neuronal functions and lead to atrophy. With the advances in brain scan technology, several distinctive tangles and plaques have been found in patients diagnosed with AD. The tangles, known as neurofibrillary tangles (NFTs), are composed of the protein Tau and the plaques are composed of the amyloid- β protein fragment. The NFTs are found deposited in the MTL in the hippocampus and entorhinal cortex². The pathological accumulation of these molecules contributes to the massive neuronal death seen in AD. Even though the exact roles of Tau and amyloid- β

are not well known, their pathological presence is well confirmed.

The Tau protein is implicated in a broader range of diseases that are classified as Tauopathies. These diseases include AD as well as frontal temporal lobe dementia, some types of Parkinson's disease, and Progressive supranuclear palsy. The Tau protein, which functions predominately in axons, is part of a class of microtubule associated proteins (MAPs)¹⁰. Tau has some known functions in the neurons but there is not much known about Tau's dynamics or structure in the neuron and how this determines its functions or role in Tauopathies.

Tau contains an N-terminal projection domain that contributes to its different proposed functions.

Tau is a MAP found predominately in the axon associated with microtubules. It has a dynamic structure and does not have a known secondary structure¹¹. The structure of Tau is important to understand in order to fully comprehend its functions in developed neurons. The N-terminus of Tau (Figure 3) is a projection domain that does not associate with the microtubule¹², and is important for proposed functions of Tau. These include a role in signaling pathways and in microtubule dynamics and stability¹³ (Figure 4).

Initial work showed that the N-terminus of Tau was important in determining microtubule spacing in microtubule bundles within the axon. Microtubules within bundles are closer to each other in the presence of Tau than with other MAPs or the absence of Tau. The N-termini of MAPs may interact with each other on adjacent microtubules to determine spacing as a function of their own length and reach. The *in vitro* study found that the microtubule spacing with Tau is consistent with spacing of microtubules in bundles found in actual axons¹⁴. Tau has a shorter N-terminal projection

domain than the MAPs found in dendrites, suggesting that microtubules in axon bundles are closer together than in dendrites.

In addition, the N-terminal projection domain has been shown to facilitate cargo delivery in the axon. Previous work has additionally shown that a region of amino acids from 2-18, known as a phosphatase-activating domain (PAD), is the necessary and sufficient region for cargo delivery¹⁵. This PAD is found in all Tau molecules and different charges on the PAD have been shown recently to have effects on the dynamics of Tau¹⁶.

The projection domain of Tau has additional effects on microtubule stability as displayed indirectly by N-terminal truncations. When the N-terminus is truncated *in vitro*, mimicking a species found pathologically in NFTs of AD brains, there is more Tau associated with tubulin. The truncated Tau is specifically associated more with acetylated tubulin and detyrosination tubulin. The detyrosinated tubulin species is a marker of microtubule stability since the PTMs occur on stable and long-lasting microtubules¹⁷. Tau is additionally known to interact with histone deacetylase 6 (HDAC6), the tubulin deacetylase, to prevent the deacetylase activity¹⁸. Although Tau plays an important role in HDAC6 activity, *in vitro* work with N-terminal truncations of Tau did not find an increase in activity of HDAC6 in those samples¹⁷. The proposed loss-of-function of Tau in inhibiting HDAC6 is potentially overcome by an increase in microtubules and stability in the presence of truncated Tau. To understand the contradiction of more acetylation in the presence of N-terminally truncated Tau, further work needs to determine if the increased tubulin modifications in the presence of N-terminally truncated Tau is the result of increased stability because Tau is more tightly bound without its N-terminus.

The Tau protein has six isoforms with common domains between the isoforms.

The gene locus for Tau on chromosome seventeen¹⁹ contains alternative splice sites resulting in six predominant isoforms (Figure 3). The primary structure of all Tau isoforms consists of an acidic N-terminus containing the PAD, two approximately central proline-rich regions, and C-terminal microtubule-binding repeats (MTBRs) (Figure 3). In the C-terminal region, isoforms of Tau either have 3 or 4 copies of a 31-amino acid microtubule-binding repeat insert. At the N-terminal region of the protein after the PAD, isoforms have 0, 1, or 2 copies of a 29-amino acid insert.

The six isoforms are named 3RS, 3RM, 3RL, 4RS, 4RM, and 4RL; reflecting the combination of alternatively spliced inserts present in the protein. 3R versus 4R signifies the presence of three or four microtubule binding repeats, while S (zero), M (one), or L (two) refers to the number of acidic inserts in the N-terminal region of the molecule. The longest isoform, 4RL, therefore contains four C-terminal microtubule-binding domains and two N-terminal acidic inserts; while the shortest isoform, 3RS, contains three C-terminal microtubule-binding domains and no N-terminal acidic inserts²⁰. In the adult brain there is approximately a 1:1 expression of 3R to 4R isoforms²¹.

Tau converts between diffusive and static states on the microtubule.

Tau is a conformationally dynamic protein with no absolute secondary structure²². This lack of secondary structure allows flexibility within the protein. It binds reversibly with the microtubule through a combination of weak interactions in the MTBR, proline-rich regions, and inter-repeat regions between MTBRs²³. The structure of Tau and the presence of multiple isoforms, although not entirely understood, are thought to have unique and overlapping roles in modulating different functions of Tau within the axon.

Despite no definite secondary structure, Tau has a proposed dynamic equilibrium on the microtubule lattice switching between a static state and a diffusive state (Figure 5). The longest and shortest isoforms, 3RS and 4RL, have different dynamic equilibria in *in vitro* studies. The 3RS isoform is found in the static state 62% of the time while 4RL is static 49% of the time²⁴. In general, the shorter isoform is more static than the longest isoform. Previous to the research presented in this study, none of the other isoforms had been characterized.

In single-molecule studies, 3RS has been found in the static state as individual molecules as well as multi-protein complexes of two to three molecules in a ratio of 1:4:2 respectively. 4RL, however, prefers single molecule binding to two-molecule static complexes in a 3:1 ratio²⁴. The function of the multi-Tau complexes is not well understood but there does not appear to be a significant number of molecules associated together in the diffusive state.

Tau adopts some known features as it transitions into the disease state.

In the disease state all isoforms of Tau are dissociated from the microtubule and prone to a pathological aggregation. The aggregates found in the disease state have accumulated modifications and are different from the physiological and reversible multi-Tau complexes observed in single molecule studies. Pathologically Tau has been found hyperphosphorylated, truncated, and associated into paired helical filaments (PHFs). Tau is subjected to a caspase-3 and calpain cleavage at distinct sites creating several different sized truncations that are found alongside full-length molecules in the PHFs^{17,25}. The PHFs are the initial component to forming NFTs that are no longer bound to the microtubules and disrupt normal axon signaling²⁶. In PHFs, Tau additionally has an

altered structure in the MTBRs that could contribute to aggregation²⁷.

Proposed models for the conversion of Tau from physiological aggregates into NFTs include stabilization of a bound state of Tau on the microtubule lattice²⁴, post translational modification like misregulated phosphorylation²⁸, mutations throughout the protein²⁹, imbalance in the ratios between the isoforms expressed³⁰, and other still developing ideas. Since studies have shown that mRNA levels of Tau are consistent between the healthy and disease states²¹, it does not appear that there is a change in the amount of Tau present causing aggregation and PHFs. Further work is needed to discern how microtubule binding is disrupted and the contribution of the different regions on aggregation.

Pathologically Tau is proposed to disrupt axonal transport and communication through the axon. Studies have suggested that since the PHFs and subsequent NFTs of Tau are no longer bound to the microtubules they can disrupt normal axon signaling and stability with the axon²⁶. Since Tau is thought to have multiple roles in the axon, it is difficult to chronicle the transition into the disease and Tau's contribution.

Alzheimer's disease is known to have disruptions in axonal transport.

Communication in a multicellular organism must be efficient yet accurate to integrate the activities of differentiated cells ranging from small organisms to coordinating the over two hundred distinct cell types in a human body. An organism must sense both external and internal stimuli and elicit fast responses ranging from pain to flight to hunger. Coordination of the senses occurs in the nervous system through its defining cell type, the neuron.

In order to maintain viable cell environments for signal propagation, neurons must

constantly exchange ion channels, synaptic proteins, pre-synaptic vesicles, organelles such as endosomes and mitochondria, plasma membrane components, and other molecules between the axon and soma³¹. Two prevalent mechanisms exist for exchanging molecules: simple diffusion and axonal transport³². Cytosolic, soluble proteins in particular move through the axoplasm with a combination of these methods based on the distance needed to travel and subcellular conditions³⁴. Simple diffusion alone is not sufficient to distribute proteins and other components down the length of the axon. Active transport, therefore, is required for the mid- to long-range distance movement of cargo along the length of the axon in both directions. The mechanism of axonal active transport turns over elements of the axoplasm such as transporting the proteins that are primarily synthesized in the soma to the distal axon (anterograde transport) and taking molecules back to the soma for recycling (retrograde transport)³³. In active transport motor proteins capable of hydrolyzing ATP, known as ATPases, transport cargo like proteins and organelles long distances along cytoskeletal filaments³².

In axons there are three main cytoskeleton polymers including actin and neurofilaments, a type of intermediate filaments. The third type are *microtubules* and are the major tracks for motor protein movement³⁵. Microtubules are dynamic polymers that provide structure and support for the axon as well as being tracks for motor proteins to move along. Microtubules are composed of heterodimers of α - and β -tubulin that associate and are added to both the plus-end of microtubules, the faster growing end extending away from the soma, and the negative-end which grows more slowly towards to soma. The tubulin heterodimers in a typical microtubule arrange into 13 protofilaments creating a structure approximately 25 nm in diameter. The microtubules polymerize most

rapidly during neurogenesis in the growth cone of developing neurons and in mature axons to develop short branch points off of stable microtubules populations. While the microtubules undergo dynamic instability during these times, most of the microtubules in the axon are strong, stable populations designated for structural support and as tracks for motor protein movement³⁶.

Within axons, different populations of stable microtubules can function in either a structural role or as a main road for motor proteins. Microtubules in a more structural role contain side extensions linking the microtubules to other cytoskeletal components like actin and neurofilaments. These projections could inhibit motor protein transport and axons have, therefore, evolved a separate population of microtubules for motor proteins to use for transport³⁷. The preference of motor proteins for certain microtubules is also influenced by significant post-translational modifications (PTMs) on tubulin that modulate motor protein transport, the motors ability to associate with the microtubule³⁸, and microtubule stability³⁹. Tubulin is subjected to acetylation, polyglutamylated, phosphorylation, and other forms of modification, particularly on its C-terminal tail. The PTMs on tubulin's C-terminal tail can influence the rate of motor protein transport as well as the propensity of motor proteins to bind the microtubule³⁸. Along with MAPs and other proteins, these PTMs help regulate axonal transport and proper cargo delivery in the axon.

Motor proteins such as kinesin transport cargo along microtubules.

Along the microtubules, molecular motors walk carrying membrane-bound vesicles as their cargo. Members of the *kinesin super family of motors (KIFs)* are primarily responsible for the anterograde motion, transporting cargo away from the cell

body (Figure 6), while cytoplasmic dynein primarily performs the anterograde motion back towards the soma³². Dynein and some members of the kinesin family are processive, meaning the motors can take multiple steps on the tubulin dimers of the microtubule before dissociating. This processivity allows for greater run lengths along the microtubule at a sufficient rate for cargo delivery to maintain the axonal environment.

The KIFs diversity of functions range from monomeric constructs to tetramers with four heads performing roles other than cargo transport⁴⁰. Certain motors within this family are more attuned to carry particular cargos and navigate the motile environment more easily³¹. Kinesin motors also have specific CNS and PNS functions, although there is overlap between what cargos are carried by a particular kinesin and with how many different kinesin types a particular cargo can associate⁴⁰. Typically adaptor proteins are involved linking KIFs or dynein with a designated cargo, increasing the combinations and specificity available for motor transport⁴¹.

Multiple different motor proteins transport cargo in neurons and often multiple motors are associated with the same cargo forming multi-motor complexes. The presence of multiple motors on the same cargo is not entirely understood but is hypothesized to help the motors navigate a complex axon environment crowded with other motors, MAPs, actin, and additional factors⁴². In some cases there may be two oppositely-directed motors on a cargo, such as dynein and kinesin. This is also hypothesized to ensure efficient cargo delivery as the dynein may engage causing the cargo to take a back step around an obstacle. The anterograde-transported vesicle can then continue forward as the kinesin motor has more space to find an available tubulin site⁴³. Other cargos may have multiple different kinesin family members on the same cargo or a combination of

KIFs and dynein^{42,44}. The combination of different motors increases how far the cargo travels on the crowded microtubule⁴⁵.

Kinesin-1 motor proteins walk along microtubules decorated with proteins and modifiers.

One of the most commonly found and studied kinesin motors in axonal transport is *kinesin-1*. The kinesin-1 motor responsible for axonal transport contains two heavy chains, forming the motor domains responsible for microtubule-binding and ATPase activity, and two light chains able to bind membrane-bound vesicles and organelles³².

The kinesin-1 motors typically step on the β -tubulin of the microtubule lattice at the interface between β -tubulin and the successive α -tubulin. The specificity for β -tubulin lends kinesin-1 to take 8 nm steps per head in a 16 nm step cycle. In the absence of crowding, kinesin ATPase activity follows Michaelis-Menten kinetics at a velocity of 600-800 nm/s, taking 12 ms per cycle at saturating ATP conditions.

Kinesin-1 hydrolyzes a single ATP per step in an ATP-cycle. In the cycle (Figure 6), the leading head is in the tightly bound state with no nucleotide in its binding site and the trailing head has a bound ATP that is hydrolyzed. With the subsequent phosphate release, the trailing head is in an ADP-bound state and has a weaker affinity for the tubulin. The head will unbind from the tubulin and, as an ATP binds to the pocket in the head that was initially the leading head, the neck linker docks and swings the trailing head forward to the next β -tubulin. At the end of the cycle, the now leading head has no nucleotide bound while the now trailing head has an ATP bound and is in a strong binding state, causing the cycle to start over⁴⁶. The ATP cycle relies on the two heads being in different nucleotide states. This allows the motor to be processive because the

trailing head can swing forward to find the next tubulin while the leading head is in a strong-binding state.

The longest and shortest isoforms of Tau can differentially modulate kinesin-1 active transport in the axon.

The MAP Tau is one such obstacle that has the ability to inhibit kinesin-1 axonal transport as it moves cargo towards the synapse⁴⁷. Tau is proposed to inhibit kinesin-1 in order to regulate the arrival of vesicles at the pre-synaptic membrane (Figure 7). Under further study, 3RS and 4RL Tau cause kinesin-1 to pause or detach at different rates (Figure 7A). In the presence of 3RS, kinesin-1 has a 50% reduced run length and was more likely to detach than in the absence of Tau. Kinesin-1 in the presence of 4RL-Tau show no change in run length but had a higher frequency of detachment compared to microtubules without Tau⁴⁷.

The different rates of kinesin-1 transport correlate with research on the dynamic behavior of 3RS and 4RL isoforms on the microtubule surface (Figure 7A). Previous studies have found that 3RS is in the static state 62% of the time. 4RL-Tau is more dynamic and found in the static state 50% of the time. The differences in dynamic equilibrium suggest that 3RS is more inhibitory of kinesin-1 due to its longer static behavior.

Tau has additional roles in axonal transport.

In addition to modulating axonal transport, Tau is also involved in signaling cascades for the delivery of kinesin-1 cargo at distinct sites along the axon. The signaling cascade includes protein phosphatase 1 and GSK3 β , a regulatory kinase. Truncations of Tau lacking either the MTBRs or MTBRs and C-terminus had a similar effects on cargo

deliver as full-length Tau by initiating the signaling cascade causing kinesin-1 to dissociate from its cargo⁴⁸. These results suggest that the N-terminus of Tau is sufficient for inducing signaling cascades and regulation of axonal transport.

The signaling importance of Tau's N-terminus has been further narrowed to a phosphatase-activating domain (PAD) in all six isoform of Tau from amino acids 2-18¹⁵. This PAD occurs before the start of the variable N-terminal acidic inserts. The PAD is sufficient and necessary to initiate signaling for cargo deliver by kinesin-1¹⁵, but is not understood whether the presence of zero, one, or two acidic inserts has additional affects on this cargo-delivery signaling cascade. Recent work has shown differential modulation of kinesin-1 by the phosphorylation state of Tau. When the negative charge of a phosphate is present at Tyrosine-18, the last amino acid of the PAD; the Tau molecule is both more diffusive and less inhibitory of kinesin-1¹⁶.

Tau does not have a known structure on the microtubule.

Since there is no confirmed structure of Tau's conformation on the microtubule, there is no clear understanding of how and why Tau transitions between the dynamic and static states. In addition, it is not clear how Tau interacts with the tubulin heterodimers of the microtubules. There are several cyro-EM studies suggesting that static Tau may lie on the microtubules across multiple protofilaments⁴⁹, along a single protofilament⁵⁰, or with density in between tubulin dimers⁵¹. Additional studies have also suggested that Tau binds at the interface between α -tubulin and β -tubulin^{52,53}. Due to Tau's dynamic nature and relatively quick transitions between static and diffusive states, however, the cryo-EM studies have low resolution and other studies have not provided a conclusive structure of static Tau.

Despite a lack of convincing structure, there is strong evidence of how regions of Tau contribute to its binding on the microtubule. Individual Tau regions have weak microtubule binding capacities but with multiple regions interacting together, Tau has a strong microtubule binding affinity. Through NMR spectroscopy studies, Tau's N-terminus is found to have little interaction with the microtubule¹². This is consistent with research suggesting that the N-terminus of Tau is a projection domain that extends away from the microtubule surface similar to those in other MAPs⁵⁴. Other work has shown that C-terminal truncations of Tau are diffuse and do not associate cleanly with microtubules⁵⁵, suggesting that the C-terminal MTBRs are necessary for microtubule-binding. In addition, Tau constructs with the MTBRs removed additionally are found predominately in supernatant fractions in pelleting assays, indicating no detectable microtubule-binding⁵⁶.

Within 4RL-Tau there are six regions found to each have a weak binding affinity to the microtubule. There is one region within each PRR, one each in microtubule-binding repeats one, two, and three; and one in the C-terminus of the protein. Together these six regions are shown in NMR to shift and adopt a different structure upon microtubule binding while other regions do not shift upon microtubule binding. The inter-repeat regions of Tau, for example, remain unbound and structurally unchanged upon microtubule binding, possibly contributing to Tau's flexibility and reversible binding on the microtubule surface¹². There is a similar shift seen in sequences in 3RS-Tau with the exception of the region in the second MTBR as 3RS does not contain that repeat-domain⁵².

Initial work on understanding regions within Tau found that the microtubule-

repeat domains of Tau, but not the C-terminus or N-terminus alone, bound to microtubules in a pelleting assay. The pelleting assays further showed that when using artificially constructed microtubule-binding repeats, two repeats had a weaker affinity for microtubules than three repeats or even four repeats, which had the strongest affinity¹¹. Along with the NMR work, these study are not entirely consistent with the kinesin-1 data or reported dynamic equilibriums of Tau where the 3RS, with one less microtubule binding repeat, spends more time in the static state on the microtubule than the isoform with four microtubule binding repeats^{24,47}.

N-terminal acidic inserts may have an effect on the dynamic equilibrium of Tau.

Since the NMR work shows that more MTBRs alone correlates with a higher affinity for the microtubule, additional features of the Tau molecules must be contributing to its ability to switch between its static and diffusive states. One such component may be the presence of the N-terminal acidic inserts. Most of the previous research on Tau has compared the 3RS with 4RL isoforms. Despite the importance of the work, there are multiple differences between the molecules that limit the ability to attribute changes in Tau dynamics to any single region of the molecule (Figure 3). In particular, 3RS has three microtubule binding repeats and no N-terminal acidic inserts while 4RL has four microtubule inserts and two N-terminal acidic inserts²¹. It is, therefore, not possible to determine whether it is the N-terminal inserts or the MTBRs influencing the dynamics and functions of the Tau isoforms.

It is important to understand differences caused by these acidic inserts because constructs with two inserts will likely have a longer projection above the microtubule that could possibly recruit more PP1 and GSK3 β for cargo delivery and signaling. The acidic

inserts, however, may also change the equilibrium of static to diffusive Tau by stabilizing the diffusive state and reducing the time a Tau is static with its PAD exposed for signaling.

Differences between the six isoforms of Tau needs to be better understood.

The research performed here proposes to examine differences in the dynamic equilibrium of Tau by comparing Tau isoforms with different N-terminal acidic insert numbers but the same number of MTBRs. The results will contribute to understanding of how the N-terminal acidic inserts may change Tau's equilibrium and, therefore, its ability to signal.

The following study will examine the difference between acidic inserts within 3-repeat Tau molecules. By keeping the microtubule-binding repeat numbers constant, this study will directly determine the role of the acidic inserts on Tau's dynamic equilibrium on the microtubule surface. The research will compare 3RL, with two N-terminal acidic inserts, to 3RS, with no N-terminal acidic inserts. This study proposes that the N-terminal acidic inserts have an effect on the equilibrium of Tau on the microtubule surface. This study proposes that the isoform with two N-terminal acidic inserts will diffuse more often and for longer than the isoform without the inserts because the additional negative charge of the 3RL isoform is able to stabilize the dynamic state.

Previous methods of data analysis may not have been sensitive enough to capture all events in single molecule assays.

The research presented here will examine the dynamic behavior of 3RS and 3RL. Previous research was able to compare the 3RS and 4RL isoforms but the methods used may not have been sensitive enough to capture short events or events that switched

between states (Figure 8). The initial work was completed by hand-selecting and characterizing events. In general, this means that very short events that were shorter than 0.5 s were too difficult to objectively characterize as static or diffusive and were, therefore, discarded. Even with strict guidelines, some events were hard to confidently categorize by eye as diffusive or static and were, therefore, not included. Finally, any event that had both static and diffusive components, which is considered a switching event, was discarded.

The research presented here developed a novel data analysis to address the limitations of the previous methods. The research aims to take away the subjectivity of hand-picking and characterizing events. In addition, the data was analyzed by running the vectors of the events through a code designed specifically to be more sensitive to short events, objectively threshold which events were static or diffusive, and categorize events that switched between states.

MATERIALS AND METHODS

Plasmid Purification and Protein Prep

Tau constructs were purified from a modified pET vector, the ampicillin-resistant pET 3d, and transformed into BL21 competent cells (Aligent cat. 230255) that were permeabilized on ice with β ME (Bio-Rad cat. 161-0710). 2-5 ng of plasmid DNA was introduced to 100 μ L of cells on ice and incubated for 30 minutes to allow the DNA to flow into the cells. The cells were heat pulsed for 30 seconds at 42°C then placed on ice for 2 minutes. Cells received 900 μ L of S.O.C. recovery media (Invitrogen cat. 15544-034, part 46-0821) and shook at 37°C, 225 rpm for 60 minutes. A range from 5-100 μ L of cells were then plated on pre-warmed LB agar (Fisher Scientific BP 9724-500) plates with 50 μ g/mL ampicillin salt (Sigma Aldrich A01566-5G) and incubated overnight at 37°C.

After 16 hours plates were removed from the incubator and one colony was selected from a plate with sufficient growth to indicate a successful transformation, but without satellite colonies or overcrowding. The colony was placed in 250 mL of LB (USB cat. 75852) with 0.1 mg/ml of ampicillin and rocked overnight at 37°C, 225 rpm. After 16 hours, the cloudy sample indicated growth and 10 mL were taken into 1 L of LB-amp at 0.1 mg/mL. The culture shook at 37°C, 225 rpm until the OD measured at λ 600 was 0.6, approximately three hours. The culture was then induced with 0.5 mM IPTG (Sigma cat. I6758-5G) and continued incubating for five hours.

At the end of five hours, the 1 L culture was spun down in a Sorvall GS-3 rotor (Thermo Fisher Scientific, Waltham, MA) for 20 min at 6,500 rpm. The supernatant was

discarded and the pellet was saved at -80°C overnight. The pellet was thawed at room temperature for 45 minutes then lysed in 40 mL of lysis buffer (3.3mL 10X BRB80 [800 mM PIPES pH 6.8 w/KOH, 10 mM EGTA, 10 mM MgSO₄], 3.3mL 10X cellytic B, 10 mM BME, 26.6mL ddH₂O, 0.2 mg/mL lysozyme, 20 µg/mL leupeptin, 1 µg/mL Pepstatin A, 10 µg/ mL Aprotinin, 1 mM PMSF, 7500 U at 250 U/µl Benzonase) and homogenized on ice until the pellet was completely broken up and the solution was uniform.

The solution containing the Tau protein was then sonicated on ice to break open the cells at a continuous pulse on for 30 seconds with 30 seconds or rest in between for 5-7 times until the solution was clear. The solution was spun in a SA600 (Thermo Fisher Scientific, Waltham, MA) rotor for 20 minutes at 4°C at 15,000 rpm. The pellet was discarded and the supernatant was placed in boiling water for 20 minutes. Most of the proteins from the cell precipitated out and were spun down in the SA600 rotor for 20 minutes at 4°C at 15,000 rpm. Tau was in the supernatant and was filtered through a 0.22 µm filter. The salutation was then applied to a Q Sepharose Fast Flow column (Sigma cat. Q1126-100mL) at 4°C at a rate of 0.5-0.8 mL/min. The flow-through containing Tau was collected and stored overnight on ice at 4°C.

The flow-through from the Q Sepharose column was applied to an SP Sepharose column (Sigma cat. S1799-100mL) at a rate of 0.5-0.8 mL/min. Tau sticks to the SP column so the flow-through was discarded. The column was then washed with BRB80 until the OD read at λ280 was zero. Once the OD reached zero, 200 mM NaCl was applied to the column to elute the Tau off the column in 1 mL fractions. The OD λ280

was recorded for each third fraction to create an elution curve. Once the elution peaked and fell back closer to zero, the salt was increased to 1 M NaCl and several fractions were collected.

Every other fraction was run on an SDS-PAGE gel and stained with Coomassie Blue stain (Figure 9A-B). Based on the samples on the gel, fractions containing Tau were pooled and placed in dialysis tubing 12-14 kDa MW cut off (Spectrum Labs cat. 132 678) and dialyzed in 2 L of 1x BRB80 overnight. After 16 hours, the dialysis tubing was placed in 1 L 1x BRB80 and dialyzed an additional 5 hours. The samples were aliquoted and flash frozen in liquid nitrogen to store long-term at -80°C. Tau concentrations were tested by a bicinchoninic acid assay (BCA assay) (Thermo Scientific prod. 23225) (Figure 9B).

Tau labeling with Alexa 488.

Tau constructs were labeled with Alexa-488 (Life Technologies cat. A10254) that uses a cysteine-maleimide-fluor linkage system. Since the 3R-Tau only has one cysteine residue in microtubule-binding repeat three, the second MTBR present in the protein (Figure 3) the constructs were singly labeled. Tau was incubated at 10x its concentration of DTT for two hours at room temperature to reduce disulfide bonds in the protein. The sample was spun through Zeba desalting columns 7k molecular weight, 2 mL volume (Thermo Scientific cat. 89889) that had been equilibrated with 1 mL of 1x BRB80 three times. The flow-through was taken and incubated with 3x Alexa-488 10 mM in DMF for two hours in the dark at room temperature. Tau-488 samples were then spun through the same type of Zeba desalting columns equilibrated the same. The flow-through was collected and aliquoted for single molecule assays and flash frozen in liquid nitrogen for

long-term storage at -80°C. Samples were run on a polyacrylamide gel to ensure no non-specific labeling occurred and that all excess dye had been filtered out (Figure 9C-D).

The concentration of Tau-488 constructs was determined by BCA assay (Figure 9D). The efficiency of labeling was measured by $\frac{\text{Concentration of label}}{\text{Concentration of protein}} * 100$ where the concentration of label was determined by absorbance at $\lambda 493$, the absorbance of the Alexa 488 dye, at different dilutions of the labeled protein. The concentration was then determined by the formula $M = (\text{OD}/\text{extinction coefficient}) * \text{dilution factor}$ using the Alexa 488 extinction coefficient.

In this study, the 3RS-Tau-488 construct stock concentration was at 92.28 μM and labeled with 49.6% efficiency. 3RL-Tau-488 stock concentration was at 23.33 μM and labeled at 97.8% efficiency.

Diffusion Assay: Tubulin Polymerization.

Tubulin purified from calf brains underwent a clarification spin at 350,000 x g at 4°C in a TLA 100 rotor in an ultracentrifuge for 20 minutes. The supernatant was removed and polymerized in the presence of 1 mM GTP at 37°C for 20 minutes. A sample of the supernatant was used to determine the OD at $\lambda 280$ to find the tubulin concentration. The polymerized microtubules were stabilized with 20 μM paclitaxel and incubated at 37°C for at least 5 minutes.

Diffusion Assay: TIRF Assay

The dynamic behavior of Tau was determined by a total internal reflection fluorescence assay (TIRF). Flow cells were constructed by adhering 0.005 mm plastic shims (Artus plastic shims, 0.005-0.125m/m) to silanized cover slips coated with PEG.

All solutions were diluted in a motility buffer (97% 1x BRB80, oxygen scavengers [3.5 mg glucose, 27 ng catalase from bovine liver, 40 ng glucose oxidase from *Aspergillus niger*], 10 mM DTT). A stock concentration of microtubules was incubated at 1:3000 with the appropriate Tau construct at 37°C for 20 minutes. All reagents were prepared fresh for imaging that day.

For imaging, anti- β III tubulin was introduced to flow cells and incubated for 5 minutes. Two washes of 0.5 mg/mL of BSA were flow-in to block spots without antibodies bound on the flow cells and allowed to bind for 2 minutes each. Between 1.2-1.5 μ M of microtubules, diluted from stock concentrations incubated with Tau, were then flowed in and incubated for 12 minutes. Tau was flowed in at a 1:3000 ratio of the microtubules, between 0.4-0.5 nM of Tau, and incubated for two minutes.

Slides were imaged with TIRF immediately on an inverted microscope (Eclipse Ti-U, Nikon) with a 100 \times plan apochromatic objective lens (1.49 NA) and auxiliary 1.5 \times magnification. Microtubules were first found and imaged with a 532 nm argon laser with an emission 605/70 band-pass filter. A 473 nm argon laser was then used to excite the Tau constructs with an emission 525/50 band-pass filter. The videos were captured by an XR/Turbo-Z camera (Stanford Photonics) with Piper Control software (v2.3.39) at a pixel resolution of 93 nm. On the microtubule field, 50 images were taken at 10 frames/second before immediately switching to image the Tau field for 1000 images at 10 frames/second.

Diffusion Assay: Data Analysis

Files from imaging were analyzed using ImageJ software, version 1.46r (National Institutes of Health, Bethesda, MD). Tau events were first confirmed by generating

kymographs, a two-dimensional representation of a movie, using the “multiple kymograph” plugin in ImageJ (Figure 8). Microtubule tracks were hand selected using the line tool and superimposed on the Tau fields to generate the kymographs (Figure 10A). Actual events were tracked using the MTrackJ plugin. Tau molecules were hand selected and followed through successive frames using MTrackJ with a single frame step between points (Figure 10B-C).

Data Analysis: MatLab

The spatial coordinates of the Tau events selected in the MTrackJ plugin were imported into MATLAB version R2016b (MathWorks, Natick, MA). A custom program was developed to distinguish between static and diffusive states for every event. The program calculated displacement of Tau particles at each time interval of 0.1 s, the frame rate during data collection, and the displacements were stored in a vector (Figure 10B-C). A sliding window analysis was performed on this displacement vector with a sliding window of size of 3 frames moving along the displacement vector.

The maximum displacement was then calculated for each window. When the maximum displacement was less than 0.3 microns that region was classified as static and when the maximum displacement was greater than 0.3 microns that region was classified as diffusive. The threshold for a static versus diffusive molecule was based on the point spread function of the fluor and minimum amount of movement able to be detected. The size of the sliding window was optimized by analyzing simulated data. In this analysis, only those tau molecules that had a time interval greater than or equal to 0.4 s were used. From the sliding window analysis; the percentage of static and diffusive events, the percentage of transitions between states, and the time spent in each state was determined.

To calculate the Diffusion Coefficient (D) and alpha value for diffusive events the mean squared displacements (MSD) were fit to the following equation (Figure 12):

$$\text{Equation 1} \quad x^2 = 4Dt^\alpha$$

where x^2 is the MSD and t is the time interval. MSD was first calculated for individual events using the following equation:

$$\text{Equation 2} \quad MSD(j) = \left(\sum_{i=1}^{L-j} (d_i, i+j)^2 \right) / L - j$$

Where j is the time interval, L is the number of values in the displacement vector and $d_i, i+j$ is the displacement between time i and $i+j$. In this way MSD was calculated for each diffusive event. Then the MSD was averaged over all particles and fit to the diffusion equation to calculate D and the alpha value. The alpha value is the exponent of the time interval in Equation 1 and is a measure of the nature of the movement of a diffusive Tau event. It describes the nature of the line in the MSD versus time graph. If the alpha value is less than 1, the line is logarithmic and suggests a sub-diffusive particle. If the value is equal to 1, the line will be linear and indicates a perfectly diffusive molecule. Finally if the value is 2, the line will be exponential and suggests directed motion.

Data Analysis: Statistics

The lifetimes of the static and diffusive events were plotted on cumulative frequency plots using Graph Pad Prism version 7.0a (GraphPad Software, Inc. La Jolla, CA). The cumulative frequency plots were analyzed with a single exponential decay and the fit values, R^2 values, were recorded as well as the dwell times, τ . The percentages of static and diffusive events were plotted as bar graph in Graph Pad Prism. Standard

deviations were calculated as:

$$\text{Equation 3} \quad \text{standard deviation} = \sqrt{(p*q*100)}$$

The percentages were compared by a two-tailed Fisher's exact test with a confidence interval of 95% through Graph Pad Prism. This statistical method allowed for comparison between the percentage of 3RS and 3RL events in the static versus diffusive states to determine statistical significance. The same process was repeated for the percentages of switching events to determine if there was statistical significance between the 3RS and 3RL rates.

RESULTS

Characterization of the 3RS and 3RL isoforms.

The expressed 3RS and 3RL isoforms were first characterized for purity. In the protein preps, the predominant product is the Tau protein running near 37 kDa on the SDS-PAGE gel. As seen in a representative gel of fractions from column elution (Figure 9A), the primary product is the 3RS protein that elutes cleanly in approximately 8-10 fractions. The concentrations of 3RS and 3RL were determined by a BCA assay run against a known Tau standard (Figure 9B). The protein concentrations were then used to determine the amount of Alexa-488 needed to incubate the protein with the dye at a 3X concentration. The SDS-PAGE gels run after labeling were stained with Coomassie Blue after imaging fluorescence on a UV light box (Figures 9C-D). Again the predominant product that was labeled is the 37 kDa Tau protein. There is also not an excess amount of dye from the labeling process as seen on the SDS-PAGE gel. Concentrations were again determined by a BCA assay and the percentage of Alexa-488 labeling was determined using the known extinction coefficient of the Alexa-488 dye. The resulting 3RS stock concentration was 92 μM , 49.6% labeled of which as labeled with Alexa-488. 3RL had a final concentration of 23 μM and was 97.8% labeled with Alexa-488.

3RS and 3RL are found more often in the static state than the diffusive state.

In the single-molecule diffusion assays, 3RS dynamics were measured in four separate experiments and 3RL dynamics were measured in three separate experiments. In each experiment data was collected from 1-2 flow cells per day and a total, across all experiments, of 14 different Tau fields for 3RS and 20 different Tau fields for 3RL. Each

field had at least 100 Tau molecules imaged over 100 seconds at 10 frames/second. In total, 555 events of 3RS were analyzed and 2168 events of 3RL (Figure 11).

The analysis showed that 3RS was in the static state 63% of the time and in the diffusive state 37% of the time. Similarly, 3RL was static 69% of the time and diffusive 31% of the time. The percentages of static Tau were not statistically significant between the two isoforms with a P-value of 0.4556 at a 95% confidence interval of $p < 0.05$ (Figures 11 and 13).

3RS and 3RL have longer static dwell times than diffusive dwell times.

Both 3RS and 3RL Tau had longer static dwell times than diffusive dwell times. Cumulative frequency plots were fit with a one-phase decay and the lifetime values were recorded as the dwell times (Figure 11). 3RS had a static dwell time of 0.53 s compared to its diffusive dwell time of 0.09 s. The static dwell time for 3RL at 0.55 s was six times longer than its diffusive dwell time at 0.12 s. The R^2 values, indicating the fit of the one-phase decay to the data, were as follows: 0.9806 for 3RS-static, 0.9816 for 3RL-static, 0.9982 for 3RS-diffusive, and 0.9994 for 3RL-diffusive (Figure 11C).

3R-Tau is more likely to switch from the diffusive state into the static state.

The novel data analysis developed here was sensitive enough to account for Tau events that switched from one state to the other. By using the sliding window analysis, the rates were determined for events that switched from the static to diffusive state and from diffusive to static state (Figures 12 and 13). Diffusive 3RS and 3RL constructs switched from diffusive to static 25% and 28% of the time, respectively. Comparatively, static 3RS molecules had a switching percentage from static to diffusive at a rate of 14%. 3RL static molecules also switched from static to diffusive at a rate of 14% (Figures 12

and 13). These percentages were not statistically significant from each at a P-value of 0.8198 at a 95% confidence interval of $p < 0.05$.

3RS and 3RL Tau are diffusive with no directed motion.

The final parameters determined from the mean-squared displacement (MSD) analysis were diffusion coefficients and alpha values for 3RS and 3RL. The diffusion coefficients were $0.072 \mu\text{m}^2/\text{s}$ for 3RS and $0.055 \mu\text{m}^2/\text{s}$ for 3RL. The alpha values were determined by plotting the MSD over time. The lines were linear, indicating an alpha value near 1, indicative of purely diffusive molecules. The alpha values were 0.970 for 3RS and 1.055 for 3RL (Figure 14).

3RS and 3RL have much shorter dwell times than previously reported.

Previous work had shown that 3RS is static 62% of the time with a static dwell times of 19.6 s and diffusive dwell times of 3.60 s (Figure 15)²⁴. The current work found 3RS was static 63% of the time with a static dwell time of 0.53 s and diffusive dwell time of 0.09 s. In order to understand the differences between the dwell times, the current data analysis was run again on the 3RS and 3RL data sets using the same thresholds as stated previously. Namely, any events less than 0.5 s (5 frames) were discarded. The results showed that the dwell times were not drastically changed (Figure 15). 3RS under the new parameters had a static dwell time of 0.63 s and a diffusive dwell time of 0.11 s. 3RL had a static dwell time of 0.68 s and a diffusive dwell time of 0.13 s.

DISCUSSION

3RS- and 3RL-Tau have similar dynamic equilibriums favoring the static state.

As shown in the results in Figures 11 and 13, both the 3RS and 3RL isoforms favor the static state at a 2:1 ratio. This is consistent with previous results using a 1:3000 ratio of 3RS to tubulin where 3RS was found to be static 62% of the time²⁴. This suggests that 3-repeat Tau isoforms overall favor the static state two-thirds of the time on the microtubule lattice.

The dwell times of 3RS and 3RL similarly showed a preference for the static state. Both isoforms had a static dwell time around 0.5 s, five times their diffusive dwell times of approximately 0.1 s (Figures 11 and 13). These results also provide an insight into the length of time Tau may be on the microtubule to perform its various functions. In general, 3-repeat Tau molecules had short dwell times that indicate rapid turnover of the molecules on the microtubule surface. Previous work had found a similar relationship where 3RS spends five times as long in the static state as the diffusive with dwell times of 19.6 s to 3.60 s respectively²⁴.

The novel data analysis method was more sensitive and captured many more short events than previous methods.

The analysis method used here was more sensitive and was able to characterize events that were not considered in the previous work (Figures 8 and 10). By using the sliding window analysis, a greater number of shorter events that were less than 0.5 s were captured. Events were also captured that either underwent a switching event or were not used previously because they were not clearly static or diffusive. Previous events were captured by hand-selecting Tau events directly from kymographs. In using kymographs,

very short events were not recorded and events where it was unclear if the molecule was diffusing were discarded.

To make sure that the dramatic differences in dwell times was not an artifact of the novel data analysis used, the data was run through the analysis again using the same thresholds as previously published. This meant any event that was less than 0.5 s was discarded (Figure 15). The results showed that 3RS under the new parameters had a static dwell time of 0.63 s and a diffusive dwell time of 0.11 s. 3RL had a static dwell time of 0.68 s and a diffusive dwell time of 0.13 s. These dwell times are still much shorter than previously reported, suggesting that the new data analysis method was indeed able to capture many events around 0.5 s that would not have been detected using previous methods of analysis.

In general, many of the Tau events were close to 0.5 s. This suggests that many Tau events are relatively short. The previous data analysis characterized events by eye as either diffusive or static. As seen in Figure 8, even with strict parameters; this can be challenging because of noise in the data collection or because these events have motion but may not be enough to categorize as diffusive or static. This data analysis used the spatial coordinates of each event and used MATLAB codes to determine the amount the event moved between frames. The subjectivity, therefore, was eliminated and events that had noise could be clearly categorized.

3R-Tau is more likely to switch from the diffusive state into the static state.

Since this study used a novel analysis method, more information was captured including the rates of switching between static and diffusive events. Previously events like the one identified in the top kymograph of Figure 8, where a Tau switched between

states, were observed on kymographs but not quantitated. Again these results favor the static state for both 3RS and 3RL. Both constructs were approximately twice as likely to switch from the diffusive state to the static state than to begin diffusing while in the static state (Figure 12). 3RS and 3RL switched favored a switch from the diffusive to the static state 25% and 28% of the time, respectively. The 3R-Tau both switched from static to diffusive 14%.

These results suggest that the 3-repeat Tau may be more stable in the static state or that it is an electrostatically more favorable conformation. In addition, the results may indicate that it is more favorable for the protein to shift from its conformation in the diffusive state into the static state. Since there is no known structure of Tau, more information is needed to understand why 3R-Tau favors the static state. A potential model for further study is that 3-repeat Tau lands on the microtubule and diffuses until it finds a suitable location. Since Tau has known signaling and other roles in the axons, it is possible Tau can land and search in the diffusive state for the appropriate location before binding.

3RS and 3RL-Tau have similar dynamic equilibriums.

This study compared 3RS and 3RL isoforms that only differ in the number of N-terminal acidic inserts. Since the percentages of static and diffusive events were not significantly different and the dwell times were comparable, these results suggest that there is no effect of the acidic inserts on Tau's equilibrium. The presence of two additional acidic inserts in 3RL did not significantly change its behavior on the microtubule compared to the 3RS as expected. The N-terminal acidic inserts may, therefore, not have a role in the dynamics of Tau but have a greater effect on its signaling

or microtubule-spacing functions^{15,14}.

Tau is a purely diffusive molecule, with no directed motion or direction bias.

The diffusion coefficients of both 3RS and 3RL show that Tau is a diffusive molecule over distances with diffusion coefficients (D) of $0.072 \mu\text{m}^2/\text{s}$ and $0.055 \mu\text{m}^2/\text{s}$, respectively (Figure 14). These D suggest that Tau is diffusing over a relatively large space each time. For comparison, the diameter of an average human microtubule is 20 nm. Since the diffusion coefficients were $72 \text{ nm}^2/\text{s}$ and $55 \text{ nm}^2/\text{s}$, this indicates a pretty diffusive molecule. These results are smaller than the previously reported diffusion coefficients of 3RS at $0.18 \mu\text{m}^2/\text{s}$ ²⁴. Since the data reported here was more sensitive to shorter diffusive events, it is likely that the diffusion coefficient reflected more short events captured that had less time to diffuse.

The alpha values for the 3-repeat isoforms were also calculated at 0.97 for 3RS and 1.06 for 3RL (Figure 14). The alpha value is determined by plotting the MSD over time. As seen in Figure 14, the plot of the line is linear with R^2 values of 0.9446 for 3RS and 0.9511 for 3RL, indicating a good fit to the line. The alpha values of 0.97 and 1.06 respectively are close to the alpha value of 1 indicating a purely diffusive molecule with no directed motion. Taken together, the alpha values and diffusion coefficients suggest that Tau is purely diffusive over distance.

FUTURE DIRECTIONS

Evaluating Isoform Specific Differences

The results of this research show that there is not a significant difference in the dynamic behavior of the 3RS and 3RL isoforms of Tau on the microtubule lattice. The next step is to use the novel data analysis methods discussed here to assess the dynamics of the remaining four isoforms. Since 3RS and 3RL had statistically similar dynamics on the microtubule, the 3RM is proposed to also favor the static state at a 2:1 rate. 3RM is additionally expected to have longer static dwell times than diffusive dwell times and switch from the diffusive state into the static state twice as often as switching from static to diffusive states.

The 4-repeat isoforms of Tau will likely have different dynamics than the 3-repeat isoforms. Based on previous work comparing 3RS and 4RL dynamics²⁴, the 4-repeat isoforms are proposed to have a 1:1 equilibrium between the static and diffusive state. The 4-repeat isoforms are proposed to similarly have longer diffusive dwell times than the 3-repeat Tau and shorter static dwell times. The individual 4-repeat isoforms are not expected to have statistically significant differences. These results would be similar to the 3-repeat work discussed above where the N-terminal acidic inserts alone do not have an effect on the dynamic equilibrium of Tau. Since the 4-repeat isoforms have more microtubule-binding repeats to interact with the tubulin of the microtubule, it is necessary to evaluate the dynamics of those isoforms to know if there is any effect of the N-terminal acidic inserts and to further understand why the 4RL isoform was more diffusive than 3RS in the previous work.

Further work is needed to characterize 3R-Tau's behavior on the microtubule.

Since 3-repeat Tau is known to form multi-Tau complexes²⁴, it is possible that the static state was longer and more frequent because multi-Tau complexes were being observed. A brightness analysis was not performed as part of the experiments presented in the current work. This assay is necessary to run in the future determine if the events observed were single or multiple molecules. In addition, binding assay could be run to determine the affinity and cooperativity of Tau for binding on the microtubule.

The analysis was stringent in the sense that any Tau event where a molecule became diffusive, static, or seemingly disappeared but the *entire* event still went on was discarded. For example, if a static Tau event was being measured through multiple frames and in one frame part of the molecule began diffusing away and the rest of the event was still static, it was assumed that there were actually at least two molecules being imaged and the entire event was not recorded. Further analysis is needed to determine the ability of 3RS and 3RL to form multi-Tau complexes and to look at the dwell times of complexes of Tau.

Since the dwell times were similar in 3RS and 3RL, it is possible that they have the same numbers of multi-Tau complexes. The rates of multi-Tau complexes also need to be studied on the remaining four isoforms; 3RM, 4RS, 4RM, and 4RL. It would, furthermore, be important to see if some isoforms are more often found as multi-Tau complexes and how that effects their transition into the disease state.

Isoform Differences on Kinesin-1 motility and signaling

Since there are not significantly differences between the 3RS and 3RL-Tau molecules, it would be interesting to look at known and proposed roles of Tau in axons to determine function-specific differences of these two isoforms. One such study would be

the motility of kinesin-1 in the presence of 3RS and 3RL to determine if the Tau isoforms inhibit kinesin-1 runs different in any significant manner. Since the dynamic equilibriums of 3RS and 3RL are similar, they may inhibit kinesin-1 similarly. Conversely, the additional acidic inserts in 3RL may impact the way the molecule interacts with kinesin-1 and show very different inhibition of the motor protein. It would, therefore, be interesting to observe kinesin-1 in single molecule motility assays, similar to those performed before^{47,58}, in the presence of 3RS or 3RL.

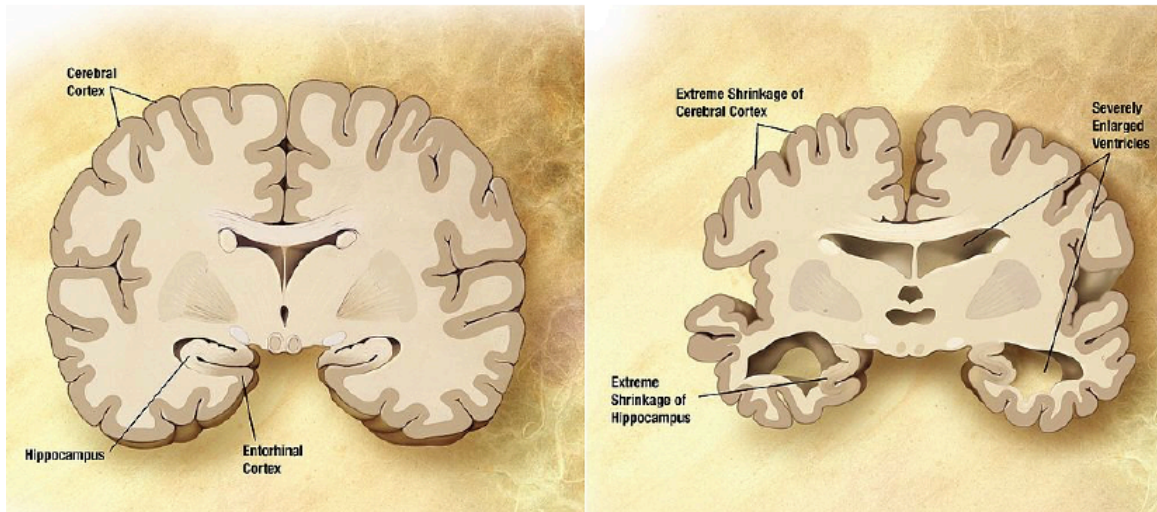
Further work could additionally look at differences in signaling between the 3RS and 3RL isoforms. The initial work on the phosphatase-activating domain of Tau used 4RL-Tau¹⁵. It would, therefore, be interesting to see if the two added N-terminal inserts effect the signaling capabilities of Tau. The PAD is the region right before the acidic inserts begin. The presence of one or two acidic inserts could, therefore, project the PAD further above the microtubule and modulate the Tau's ability to signal. These N-terminal acidic inserts may have an effect on recruiting kinases to initiate signaling for cargo delivery and other functions. One way to see the effect of the inserts on signaling would be to express different isoforms of Tau in cells and look at the levels of phosphorylation on kinesin-1. This would indirectly show a change in signaling and recruitment of GSK3 β and PP1 in the presence of different isoforms.

CONCLUSION

Since there were not any statistical differences in the dynamic equilibriums of 3RS and 3RL, it is possible that there are functional differences based on the N-terminal acidic inserts. Further studies are needed to determine if the isoforms have complementary roles in signaling, microtubule spacing, and kinesin-1 inhibition. In addition, more work is needed to compare how all six constructs function and to begin understanding why there are six isoforms in the adult brain. Finally, these studies could be used to determine how Tau develops into the pathologies found in neurodegenerative diseases and potential therapeutic targets.

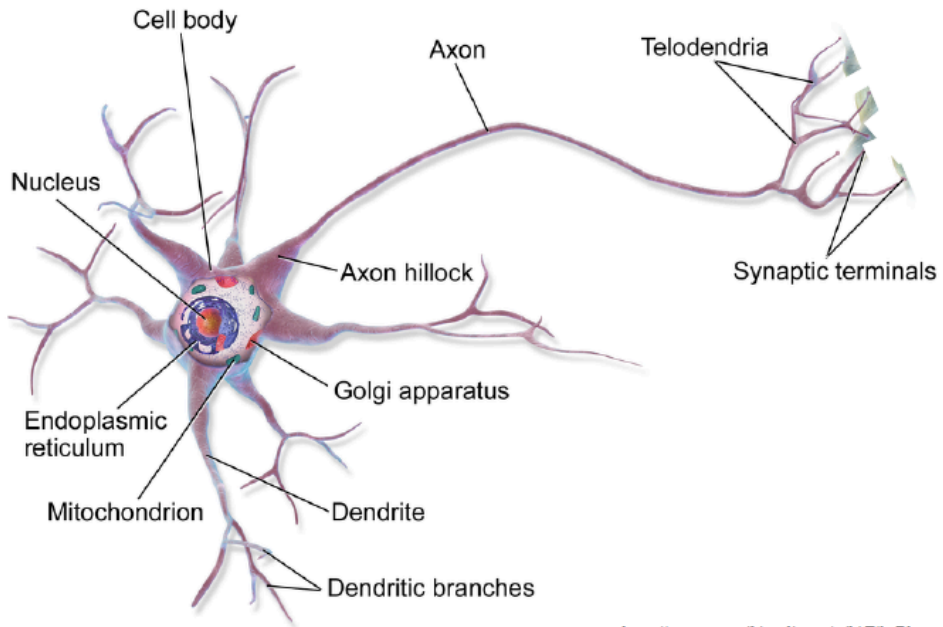
The research described here is an important first step to answer many of these questions and to understanding the Tau protein. First, the novel data analysis tools developed here provided a more detailed and thorough characterization of the 3RS and 3RL Tau proteins. These methods can be applied to other single molecule studies assessing the dynamics of Tau and other MAPs. Secondly, this study looked at two Tau isoforms that were previously not characterized relative to each other. By examining 3-repeat isoforms, the work here begins to understand the role of the N-terminal acidic inserts on the dynamics of Tau.

Figure 1: Necrosis is found in different regions of the brain in AD. Patients with Alzheimer's disease have presented with necrosis in multiple different brain regions including the the limbic system, medial temporal lobe, frontal temporal lobe, and hippocampus. In these images taken by magnetic resonance imaging (MRI) are overlays of atrophy seen in AD and amnesic MCI patients. The blue shows areas of gray matter atrophy and red shows white matter atrophy.



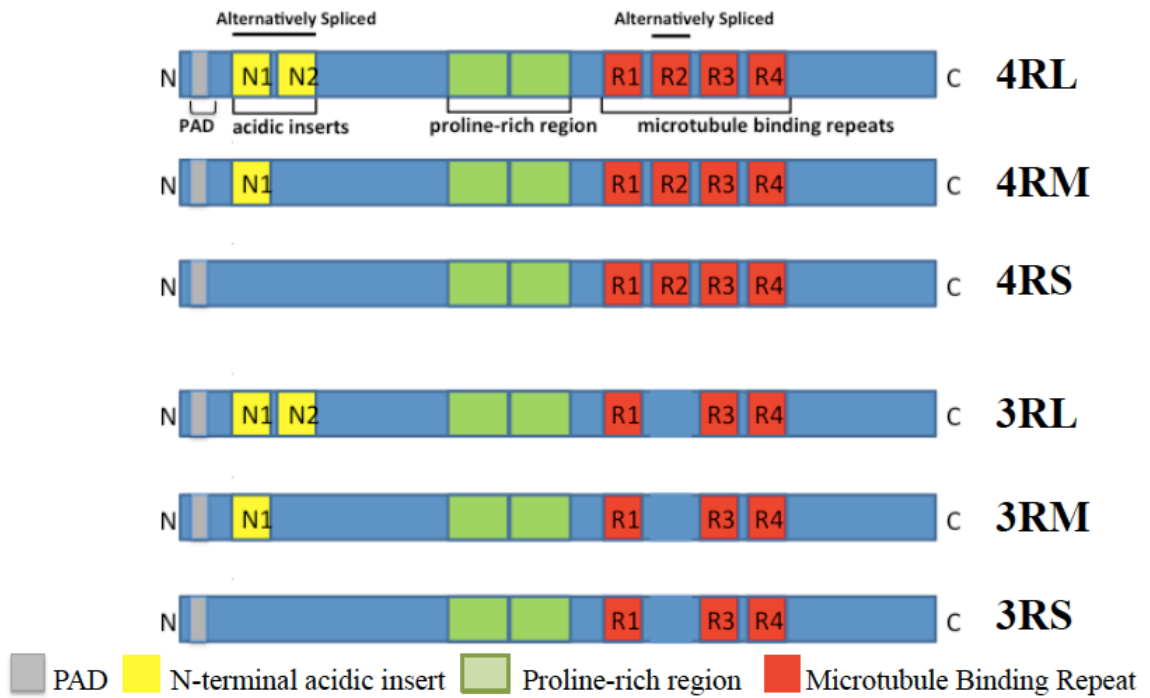
https://commons.wikimedia.org/wiki/File:Alzheimer%27s_disease_brain_comparison.jpg

Figure 2: Neurons are a highly polarized cell in the brain. Neurons have extension off of their cell body, also known as a soma. The neuron receives the signal from the previous neuron at its dendrites, the shorter branched extensions. The signal is then sent down the axon, the longer extension, to the dendrites of the next neuron. Additional features of neurons have roles in propagating the signal and maintaining the polarity of the cell.



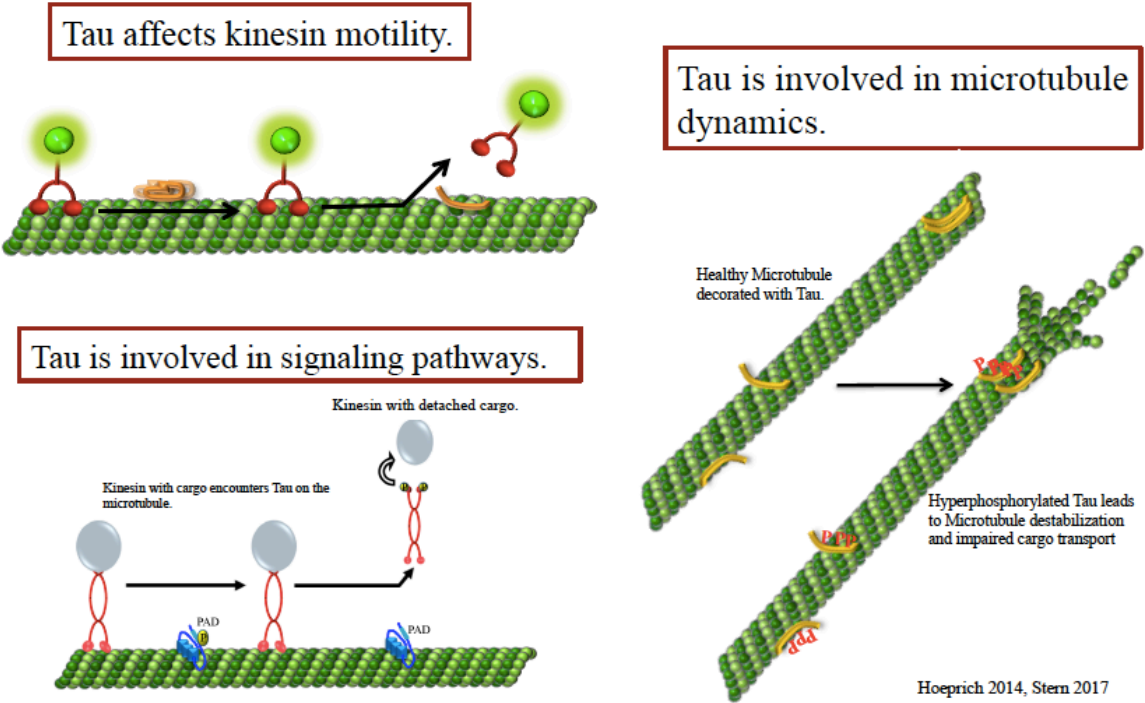
https://commons.wikimedia.org/wiki/File:Blausen_0657_MultipolarNeuron.png

Figure 3: Tau has six isoforms alternatively spliced from the same gene on chromosome 17. The Tau isoforms have common features including a phosphatase-activating domain, two Proline-rich regions, and C-terminal microtubule-binding repeats. The isoforms differ by the presence of zero, one, or two N-terminal acidic inserts and the presence or absence of microtubule-binding repeat 2.



Himmler et al (1989), Goedert et al (1989)

Figure 4: Tau is involved in kinesin-1 inhibition, microtubule stabilization, and signaling pathways. Tau has multiple roles in the axon. It has been shown to interact with motor proteins like kinesin-1, is involved in microtubule dynamics and stability, and, through its PAD, is part of signaling pathways.



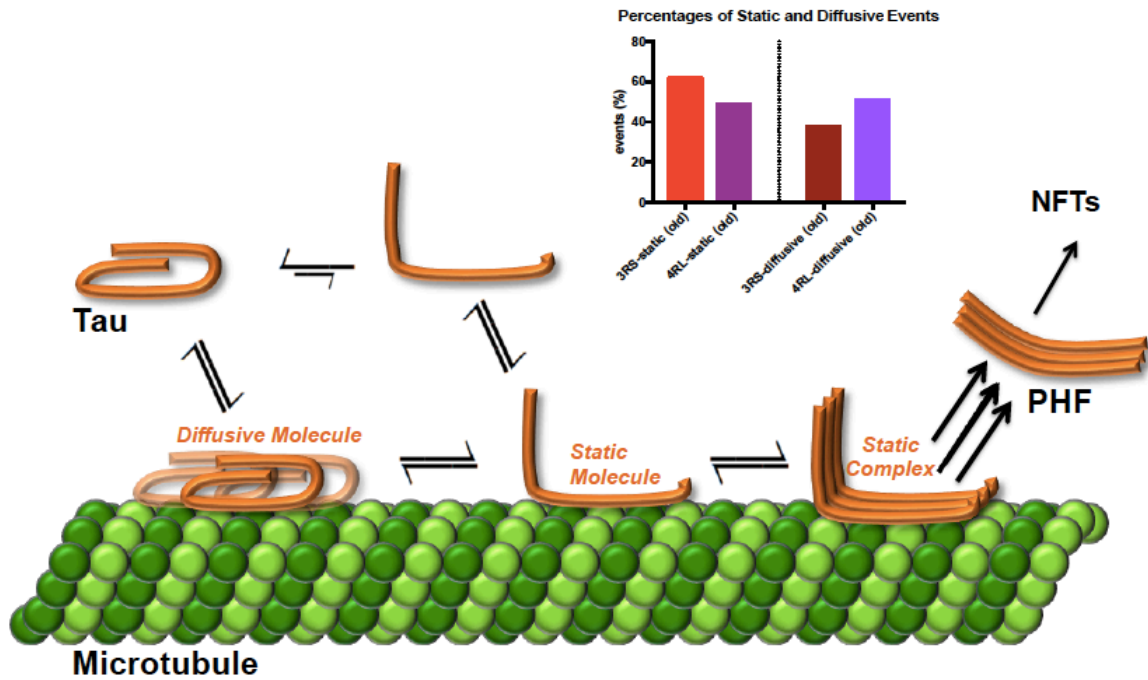


Figure 5: A proposed model shows how Tau is a conformationally dynamic protein converting between a static and diffusive state on the microtubule. Tau is a conformationally dynamic protein. The actual conformation of Tau in either state is unknown. The above model shows some suggested forms where Tau switches from a closed conformation in the diffusive state to an open conformation in the static state. It is thought that Tau in the static state can form multi-Tau complexes. In AD and other Tauopathies, Tau molecules aggregate when they become hyperphosphorylated and are truncated. These aggregated develop into paired-helical filaments (PHF) and eventually neurofibrillary tangles (NFTs).

McVicker 2014 *Cytoskeleton*

Figure 6: Kinesin-1 hydrolyzes ATP with each step it takes. During kinesin-1's ATP cycle, the leading head is in the tightly bound state with no nucleotide in its binding site and the trailing head has a bound ATP that is hydrolyzed (1). When the phosphate is released, the trailing head is in an ADP-bound state and has a weaker affinity for the tubulin. The head will unbind from the tubulin (2). An ATP binds in the initial leading head and the neck linker docks, swinging the trailing head forward to the next β -tubulin (3). At the end of the cycle, the now leading head has no nucleotide bound while the now trailing head has an ATP bound and is in a strong binding state, causing the cycle to start over.

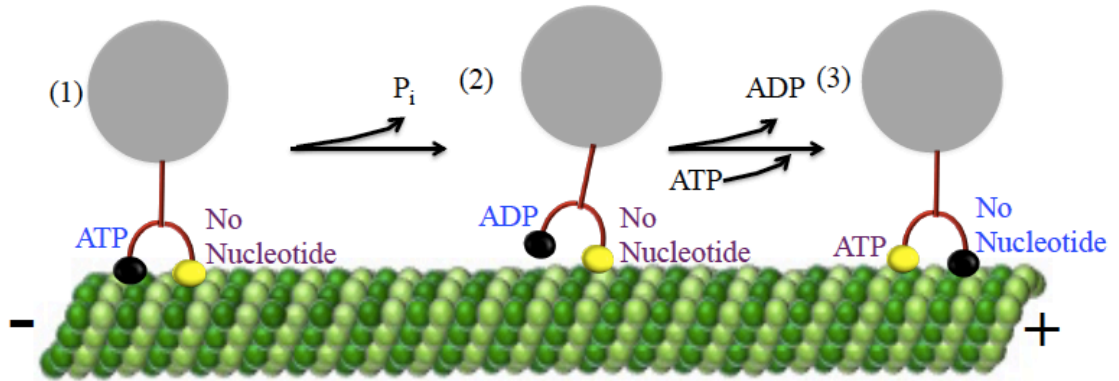
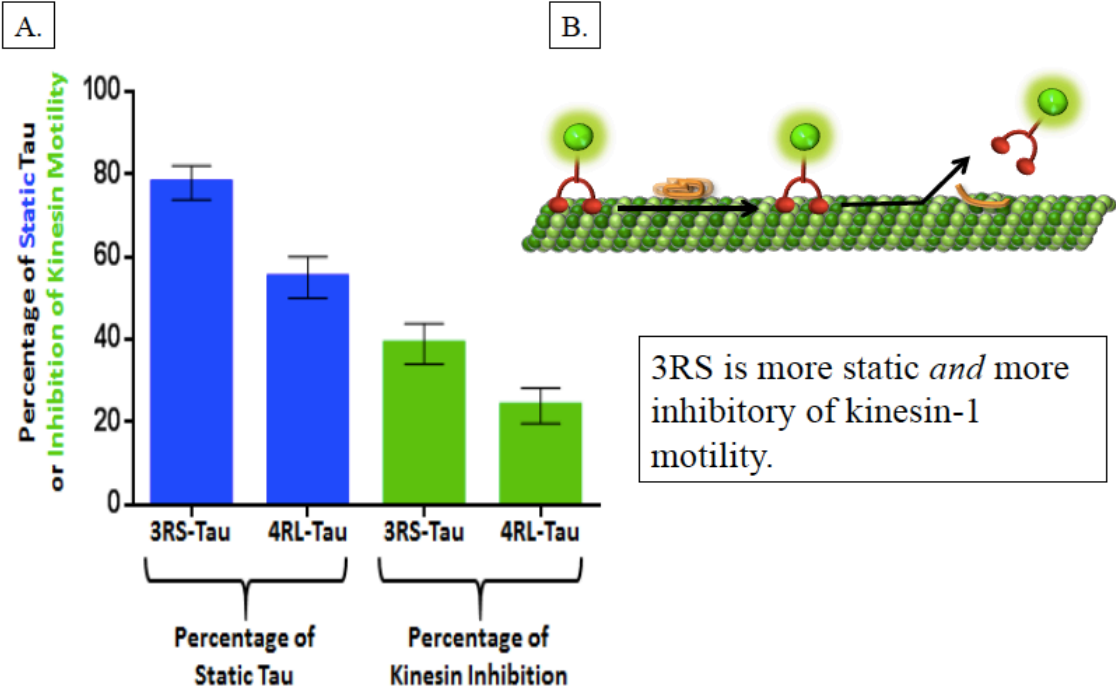


Figure 7: Kinesin-1 is inhibited by Tau. (A) Kinesin-1 is more inhibited by 3RS Tau than 4RL. Since 3RS is more static than 4RL, these results correlate. Namely, kinesin-1 is more inhibited by the more static Tau isoform. In the model (B) a kinesin motor pauses and detaches in the presence of a Tau molecule.



Greg Hoeplich
Derrick McVicker

Figure 8: Sample kymographs of Tau show molecules in different states. Tau can be diffusive (blue arrow), static (green arrow) or can switch between static and diffusive (orange arrow). The novel data analysis used here was sensitive enough to capture short events (red arrows) that were difficult to characterize and, therefore, not used in previous analyses.

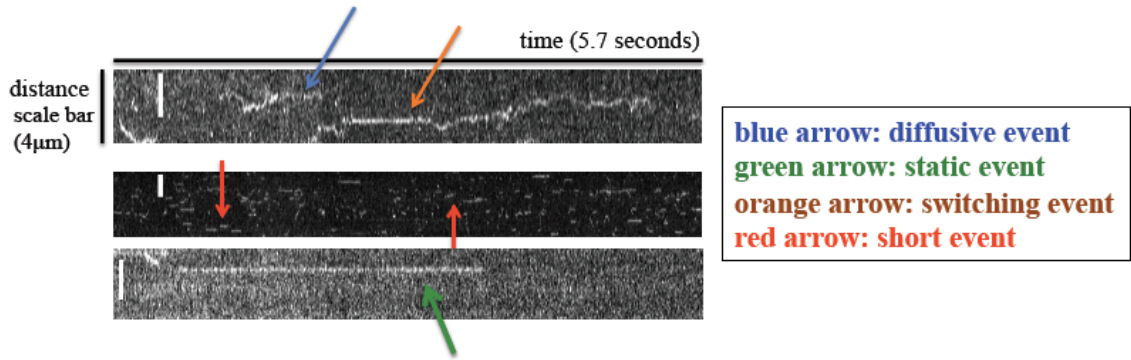
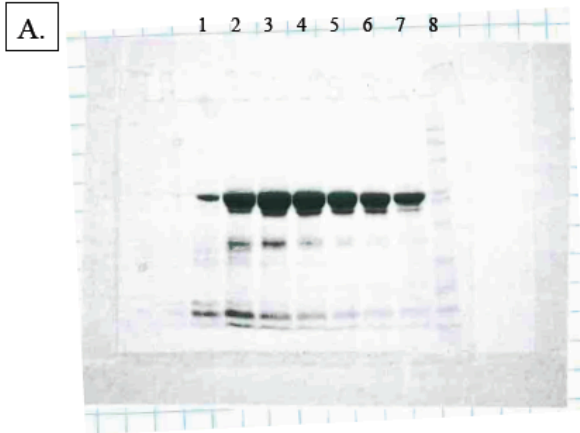
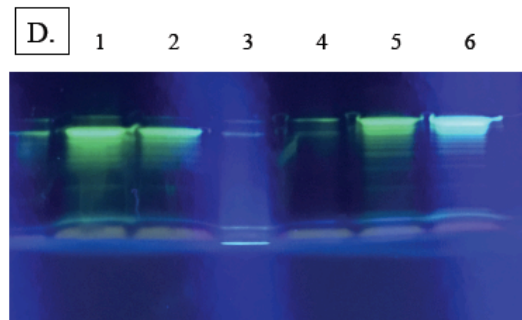
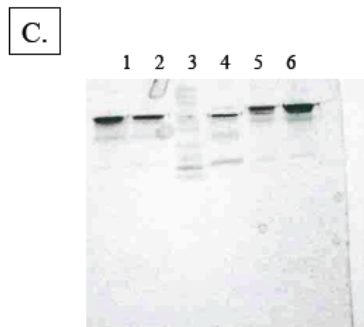


Figure 9: Characterization of the protein prep and labeling of the 3R-isoforms. Representative protein preps from 3RS show a predominant product around 37 kDa (A) that is consistent with how Tau runs on a denaturing polyacrylamide gel. Lanes 1-7 are every other fraction from column elution, lane 8 is the ladder. The concentrations of the purified constructs were determined by a BCA assay run against a known Tau construct as the standard. The dye concentration was determined using the extinction coefficient of Alexa 488 (B). The 3RS and 3RL constructs were labeled with Alexa-488. The Tau product running around 37 kDa is again the predominant product that was labeled in the Coomassie Blue stain (C). The labeled constructs were run to ensure no excess dye or off-target labeling occurred (D). Concentrations were again determined by a BCA assay against a known Tau concentration as a standard. The percentage of labeling was determined using the extinction coefficient of Alexa-488.



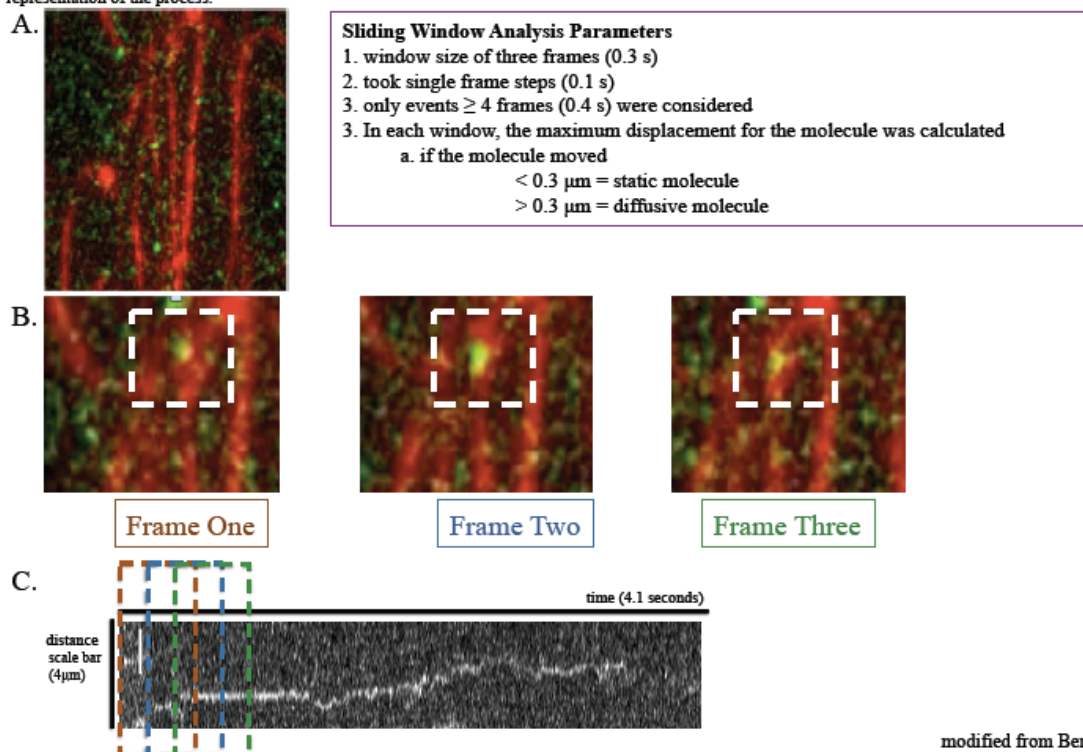
B.

	Concentration	Labeling Percentage
3RS-488	92 μ M	49.6%
3RL-488	23 μ M	97.8%

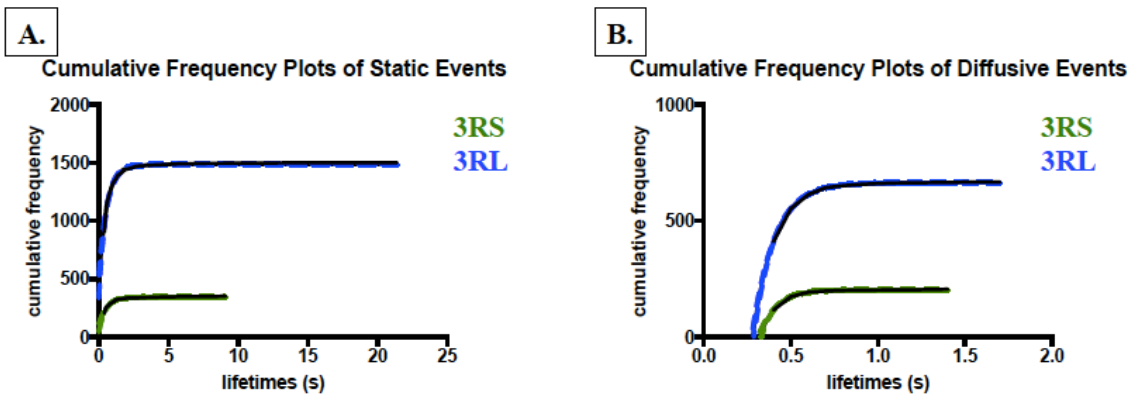


1	2	3	4	5	6
3RS-488	3RS-488	ladder	3RL unlabeled	3RL-488	3RL-488
10 μ M	5 μ M	10 μ M	10 μ M	5 μ M	10 μ M

Figure 10: A sliding window analysis was used to characterize Tau events. The novel data analysis uses a sliding window of three frames with single frame steps on molecules selected from a video of Tau on microtubules (A.) to assess the position of the Tau molecule from frame to frame (B.). The sliding window analysis is sensitive enough to capture both very short events and events that switch between the static and diffusive states. The kymograph represents the sliding window analysis from frame to frame over an entire event. Note: the events were not characterized from kymographs. (C.) is meant as a visual representation of the process.



modified from Berger Lab



C.

	static	static R ²	diffusive	diffusive R ²	static dwell time	diffusive dwell time	number of events
3RS	63%	0.9806	37%	0.9982	0.53 s	0.09 s	555
3RL	69%	0.9816	31%	0.9994	0.55 s	0.12 s	2168

Figure 11: 3RS and 3RL favor the static state at a 2:1 ratio and have longer static dwell times than diffusive dwell times. The cumulative frequency plots of the static events show that lifetimes last longer in the static state (A) than diffusive state (B). The cumulative frequency plots were fit with a single exponential decay to determine dwell times (lifetimes). The fit of the line, R² values, are reported as well (C). There is no significance in the ratios of static to diffusive events between 3RS and 3RL at a 95% confidence interval (P-value: 0.4556).

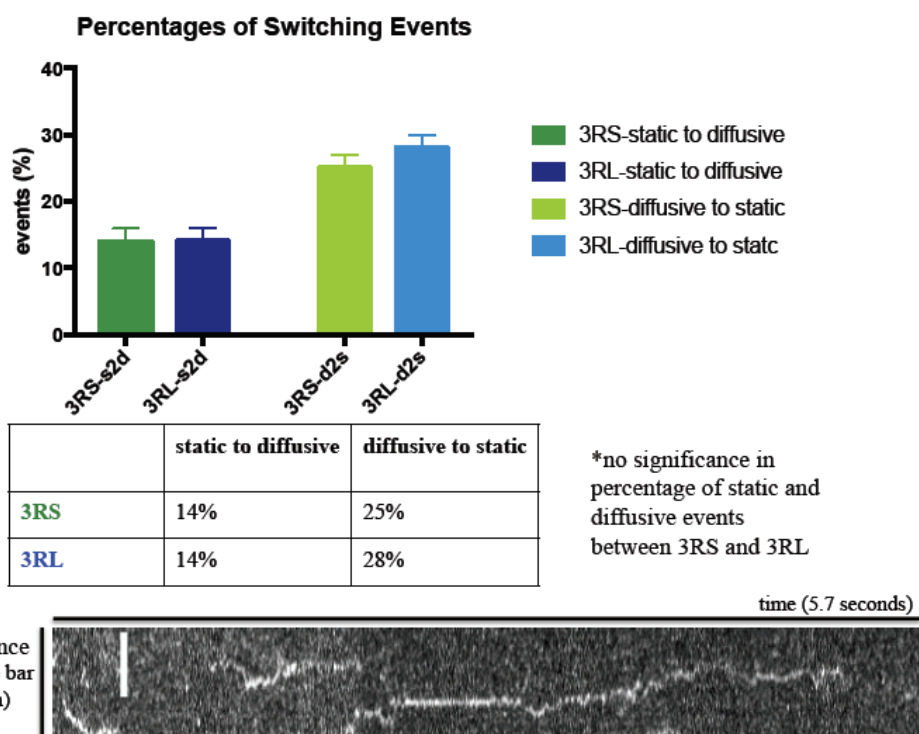


Figure 12: 3RS and 3RL switch more often from the diffusive to static. 3RS and 3RL are more likely to switch from the diffusive state into the static state than move from static into diffusive. These percentages of switches are not significant between 3RS and 3RL at a 95% confidence interval (P-value: 0.8198)

Percentages of Static and Diffusive Events

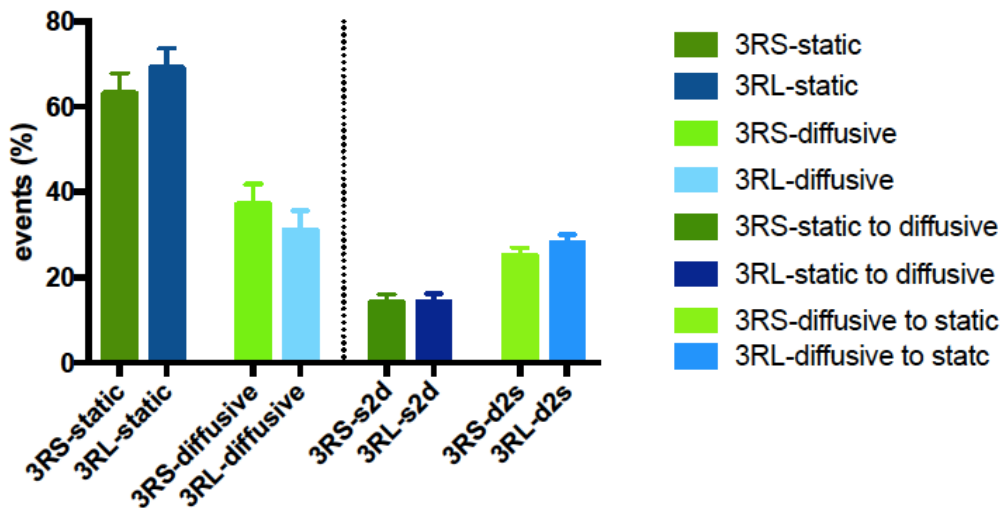
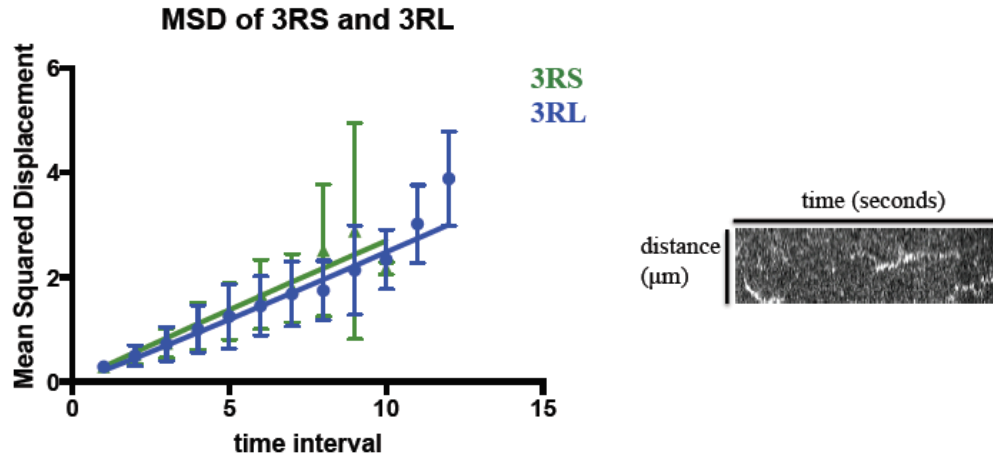


Figure 13: 3RS and 3RL favor the static state at a 2:1 ratio. There is no significance in the percentages of the 3RS and 3RL at a 95% confidence interval (P-value: 0.4556). Both isoforms switch states 25% of the time and are twice as likely to switch from diffusive to state than from static to diffusive. There is no significant difference in the switching percentages between the 3RS and 3RL isoforms (P-value: 0.8198).

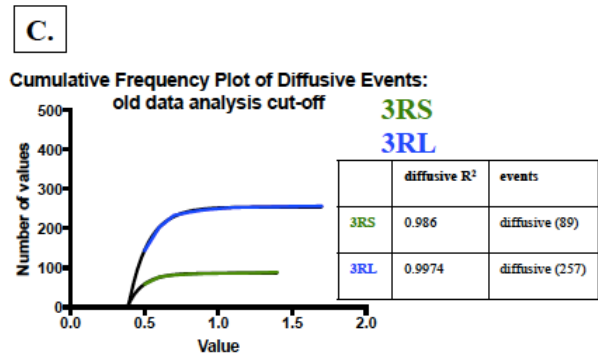
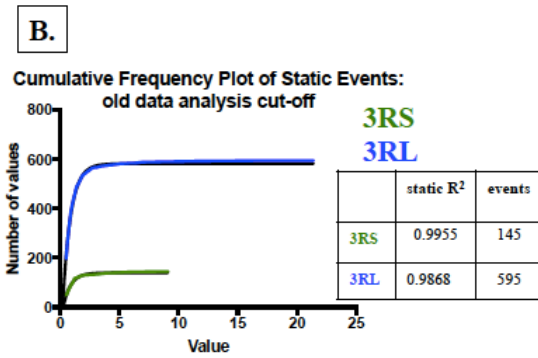
Figure 14: 3RS and 3RL in the diffusive state have no directed motion. Both 3RS and 3RL diffuse over short distances based on their low diffusion coefficients. The alpha values for both isoforms are close to 1, indicating that they are diffusive and do not have directed motion.



	diffusion coefficient	alpha value	R-squared
3RS	0.072 $\mu\text{m}^2/\text{s}$	0.97	0.9446
3RL	0.055 $\mu\text{m}^2/\text{s}$	1.06	0.9511

Figure 15: 3RS has much shorter dwell times in this data analysis than previous ones. (A) Previously, the dwell times of 3RS were reported at 19.6 s for static 3RS and 3.60 s for diffusive 3RS. (B-C) In order to understand differences in dwell times from the previous and current work, the current work was re-analyzed at a threshold of 5 frames, where events had to last at least 5 frames (0.5 s) to be considered, the same cut-off as the old analysis. (D) The dwell times were

A.	3RS (old)	3RS (new)	4RL (old)	3RL (new)
static events	62%	63%	49%	69%
static dwell times	19.6 s	0.53 s	5.80 s	0.55 s
diffusive dwell times	3.60 s	0.09 s	3.87 s	0.12 s
static dwell times (old thresholds)		0.63 s		0.68 s
diffusive dwell times (old thresholds)		0.11 s		0.13 s



McVicker *et al.* 2014

WORKS CITED

1. Alzheimer Association. 2016 Alzheimer's Disease Facts and Figures. *Alzheimer's Dement.* 2016 **12**, 1–80 (2016).
2. Suri, S., Topiwala, A., Mackay, C. E., Ebmeier, K. P. & Filippini, N. Using structural and diffusion magnetic resonance imaging to differentiate the dementias. *Curr. Neurol. Neurosci. Rep.* **14**, 475 (2014).
3. de Leeuw, F.-E., Korf, E., Barkhof, F. & Scheltens, P. White matter lesions are associated with progression of medial temporal lobe atrophy in Alzheimer disease. *Stroke.* **37**, 2248–52 (2006).
4. Hebert, L. E., Weuve, J. & Evans, D. A. Alzheimer disease in the United States (2010 – 2050) estimated using the 2010 census. *Am. Acad. Neurol.* **158**, (2013).
5. Association, A. P. *Diagnostic and Statistical Manual of Mental Disorders, Fifth Edition: DSM-5.* (American Psychiatric Publishing, 2013).
6. Agosta, R., Pievani, M., Sala, S., Geroldi, C., Galluzzi, S., Frisoni, G. B. & Filippi, M. White Matter Damage in Alzheimer Disease and Its Relationship to Gray Matter Atrophy. *Radiology* **258**, 853–863 (2011).
7. de la Monte, S. Quantitation of cerebral atrophy in preclinical and end-stage Alzheimer's disease. *Ann. Neurol.* **25**, 450–459 (1989).
8. Oishi, K. & Lyketsos, C. G. Alzheimer's disease and the fornix. *Front. Aging Neurosci.* **6**, 1–9 (2014).
9. Jobst, K., Smith, A., Szatmari, M., Esiri, M., Jaskowski, A., Hindley, N., McDonald, B. & Molyneux, A. Rapidly progressing atrophy of medial temporal lobe in Alzheimer's disease. *Lancet* **343**, 829–830 (1994).
10. Cleveland, D. W., Hwo, S. Y. & Kirschner, M. W. Purification of tau, a microtubule-associated protein that induces assembly of microtubules from purified tubulin. *J. Mol. Biol.* **116**, 207–25 (1977).
11. Butner, K. A. & Kirschner, M. W. Tau Protein Binds to Microtubules through. *J. Cell Biol.* **115**, 717–730 (1991).
12. Kadavath, H., Jaremko, M., Jaremko, J., Biernat, J., Mandelkow, E. & Zweckstetter, M. Folding of the Tau Protein on Microtubules. *Angew. Chemie - Int. Ed.* **54**, 10347–10351 (2015).
13. Drechsel, D. N., Hyman, a a, Cobb, M. H. & Kirschner, M. W. Modulation of the dynamic instability of tubulin assembly by the microtubule-associated protein tau. *Mol. Biol. Cell* **3**, 1141–54 (1992).
14. Chen, J., Kanai, Y., Cowan, N. J. & Hirokawa, N. Projection domains of MAP2 and tau determine spacings between microtubules in dendrites and axons. *Nature* **360**, 674–677 (1992).
15. Kanaan, N. M., Morfini, G. a, LaPointe, N. E., Pigino, G. F., Patterson, K. R., Song, Y., Andreadis, A., Fu, Y., Brady, S. T. & Binder, L. I. Pathogenic forms of tau inhibit kinesin-dependent axonal transport through a mechanism involving activation of axonal phosphotransferases. *J. Neurosci.* **31**, 9858–68 (2011).
16. Stern, J., Lessard, D., Hoepflich, G., Morfini, G. & Berger, C. Phospho-regulation of Tau Modulates Inhibition of Kinesin-1 Motility. *Mol. Biol. Cell* **18**, 1–16 (2017).

17. Derisbourg, M., Leghay, C., Chiappetta, G., Fernandez-Gomez, F.-J., Laurent, C., Demeyer, D., Carrier, S., Buée-Scherrer, V., Blum, D., Vinh, J., Sergeant, N., Verdier, Y., Buée, L. & Hamdane, M. Role of the Tau N-terminal region in microtubule stabilization revealed by new endogenous truncated forms. *Sci. Rep.* **5**, 9659 (2015).
18. Perez, M., Santa-Maria, I., De Barreda, E. G., Zhu, X., Cuadros, R., Cabrero, J. R., Sanchez-Madrid, F., Dawson, H. N., Vitek, M. P., Perry, G., Smith, M. A. & Avila, J. Tau - An inhibitor of deacetylase HDAC6 function. *J. Neurochem.* **109**, 1756–1766 (2009).
19. Neve, R. L., Harris, P., Kosik, K. S., Kurnit, D. M. & Donlon, T. a. Identification of cDNA clones for the human microtubule-associated protein tau and chromosomal localization of the genes for tau and microtubule-associated protein 2. *Brain Res.* **387**, 271–80 (1986).
20. Goode, B. L., Chau, M., Denis, P. E. & Feinstein, S. C. Structural and functional differences between 3-repeat and 4-repeat tau isoforms. Implications for normal tau function and the onset of neurodegenerative disease. *J. Biol. Chem.* **275**, 38182–9 (2000).
21. Goedert, M., Spillantini, M. G., Rutherford, D. & Crowther, R. A. Multiple Isoforms of Human Microtubule-Associated Protein Tau : Sequences and localization in Neurofibrillar Tangles of Alzheimer ' s Disease is found. **3**, 519–526 (1989).
22. Jeganathan, S., von Bergen, M., Brütlich, H., Steinhoff, H.-J. & Mandelkow, E. Global hairpin folding of tau in solution. *Biochemistry* **45**, 2283–93 (2006).
23. Goode, B. L. & Feinstein, S. C. Identification of a novel microtubule binding and assembly domain in the developmentally regulated inter-repeat region of tau. *J. Cell Biol.* **124**, 769–82 (1994).
24. McVicker, D. P., Hoepflich, G. J., Thompson, A. R. & Berger, C. L. Tau interconverts between diffusive and stable populations on the microtubule surface in an isoform and lattice specific manner. *Cytoskeleton (Hoboken)*. **71**, 184–94 (2014).
25. Novak, M., Kabat, J. & Wischik, C. M. Molecular characterization of the minimal protease resistant tau unit of the Alzheimer's disease paired helical filament. *EMBO J.* **12**, 365–370 (1993).
26. Grundke-iqbal, I., Iqbal, K., Tung, Y., Zaidi, M. S. & Wisniewski, H. M. Microtubule-associated Protein Tau. **4**, 6084–6089 (1986).
27. Jeganathan, S., Bergen, M. Von, Mandelkow, E. & Mandelkow, E. The Natively Unfolded Character of Tau and Its Aggregation to Alzheimer-like. **2**, 10526–10539 (2008).
28. Hashiguchi, M. & Hashiguchi, T. Kinase-kinase interaction and modulation of Tau phosphorylation. *Int. Rev. Cell Mol. Biol.* **300**, 121–160 (2013).
29. Brunden, K. R., Trojanowski, J. Q. & Lee, V. M.-Y. Advances in tau-focused drug discovery for Alzheimer's disease and related tauopathies. *Nat. Rev. Drug Discov.* **8**, 783–93 (2009).
30. Panda, D., Samuel, J. C., Massie, M., Feinstein, S. C. & Wilson, L. Differential regulation of microtubule dynamics by three- and four-repeat tau: implications for

- the onset of neurodegenerative disease. *Proc. Natl. Acad. Sci. U. S. A.* **100**, 9548–53 (2003).
31. Sgro, A. E., Bajjalieh, S. M. & Chiu, D. T. Single-axonal organelle analysis method reveals new protein-motor associations. *ACS Chem. Neurosci.* **4**, 277–84 (2013).
 32. Brady, S. T. Molecular motors in the nervous system. *Neuron* **7**, 521–33 (1991).
 33. Hoffman, P. N. & Lasek, R. THE SLOW COMPONENT OF AXONAL TRANSPORT Identification of Major Structural Polypeptides of the Axon and Their Generality among Mammalian Neurons Labeling Axonally Transported Polypeptides in Rat Ventral Motor Neurons and Cat Dorsal Root Determining the Dis. **66**, 351–366 (1975).
 34. Scholz, T. & Mandelkow, E. Transport and diffusion of Tau protein in neurons. *Cell. Mol. Life Sci.* **71**, 3139–50 (2014).
 35. Kreutzberg, G. W. Neuronal dynamics and axonal flow. IV. Blockage of intra-axonal enzyme transport by colchicine. *Proc. Natl. Acad. Sci. U. S. A.* **62**, 722–8 (1969).
 36. Dent, E. W., Callaway, J. L., Szebenyi, G., Baas, P. W. & Kalil, K. Reorganization and movement of microtubules in axonal growth cones and developing interstitial branches. *J. Neurosci.* **19**, 8894–908 (1999).
 37. Miller, R. H., Lasek, R. J. & Katz, M. J. Preferred microtubules for vesicle transport in lobster axons. *Science* **235**, 220–2 (1987).
 38. Sirajuddin, M., Rice, L. M. & Vale, R. D. Regulation of microtubule motors by tubulin isotypes and post-translational modifications. *Nat. Cell Biol.* **16**, 335–44 (2014).
 39. Sudo, H. & Baas, P. W. Acetylation of microtubules influences their sensitivity to severing by katanin in neurons and fibroblasts. *J. Neurosci.* **30**, 7215–26 (2010).
 40. Okada, Y., Yamazaki, H., Sekine-Aizawa, Y. & Hirokawa, N. The neuron-specific kinesin superfamily protein KIF1A is a unique monomeric motor for anterograde axonal transport of synaptic vesicle precursors. *Cell* **81**, 769–80 (1995).
 41. Hirokawa, N. & Takemura, R. Kinesin superfamily proteins and their various functions and dynamics. *Exp. Cell Res.* **301**, 50–9 (2004).
 42. Hirokawa, N., Niwa, S. & Tanaka, Y. Molecular motors in neurons: transport mechanisms and roles in brain function, development, and disease. *Neuron* **68**, 610–38 (2010).
 43. Dahlstrom, A. B., Pfister, K. K. & Brady, S. T. The axonal transport motor ‘kinesin’ is bound to anterogradely transported organelles: quantitative cytofluorimetric studies of fast axonal transport in the rat. *ACTA Physiol. Scand.* **141**, 469–476 (1991).
 44. Xu, J., King, S. J., Lapierre-Landry, M. & Nemeč, B. Interplay between velocity and travel distance of kinesin-based transport in the presence of tau. *Biophys. J.* **105**, L23-5 (2013).
 45. Vershinin, M., Carter, B. C., Razafsky, D. S., King, S. J. & Gross, S. P. Multiple-motor based transport and its regulation by Tau. *Proc. Natl. Acad. Sci. U. S. A.* **104**, 87–92 (2007).
 46. Verbrugge, S., Lansky, Z. & Peterman, E. J. G. Kinesin’s step dissected with

- single-motor FRET. *Proc. Natl. Acad. Sci. U. S. A.* **106**, 17741–6 (2009).
47. Dixit, R., Ross, J. L., Goldman, Y. E. & Holzbaaur, E. L. F. Differential regulation of dynein and kinesin motor proteins by tau. *Science* **319**, 1086–1089 (2008).
 48. Lapointe, N. E., Morfini, G., Pigino, G., Gaisina, I. N., Alan, P., Binder, L. I. & Brady, S. T. Transport : Implications for Filament Toxicity. *J. Neurosci.* **87**, 440–451 (2009).
 49. Santarella, R. a., Skiniotis, G., Goldie, K. N., Tittmann, P., Gross, H., Mandelkow, E. M., Mandelkow, E. & Hoenger, A. Surface-decoration of microtubules by human tau. *J. Mol. Biol.* **339**, 539–553 (2004).
 50. Al-Bassam, J., Ozer, R. S., Safer, D., Halpain, S. & Milligan, R. a. MAP2 and tau bind longitudinally along the outer ridges of microtubule protofilaments. *J. Cell Biol.* **157**, 1187–1196 (2002).
 51. Kar, S., Fan, J., Smith, M. J., Goedert, M. & Amos, L. a. Repeat motifs of tau bind to the insides of microtubules in the absence of taxol. *EMBO J.* **22**, 70–77 (2003).
 52. Kadavath, H., Hofele, R. V, Biernat, J., Kumar, S., Tepper, K., Urlaub, H., Mandelkow, E. & Zweckstetter, M. Tau stabilizes microtubules by binding at the interface between tubulin heterodimers. *Proc Nat Acad Sci USA* **112**, 7501–7506 (2015).
 53. Cabantous, S., Nguyen, H. B., Pedelacq, J.-D., Koraïchi, F., Chaudhary, A., Ganguly, K., Lockard, M. a, Favre, G., Terwilliger, T. C. & Waldo, G. S. A new protein-protein interaction sensor based on tripartite split-GFP association. *Sci. Rep.* **3**, 2854 (2013).
 54. Gustke, N., Trinczek, B., Biernat, J., Mandelkow, E. M. & Mandelkow, E. Domains of tau protein and interactions with microtubules. *Biochemistry* **33**, 9511–9522 (1994).
 55. Preuss, U., Biernat, J., Mandelkow, E. M. & Mandelkow, E. The ‘jaws’ model of tau-microtubule interaction examined in CHO cells. *J. Cell Sci.* **110 (Pt 6)**, 789–800 (1997).
 56. Morfini, G., Pigino, G., Mizuno, N., Kikkawa, M. & Brady, S. T. Tau Binding to Microtubules Does Not Directly Affect Microtubule-Based Vesicle Motility. *J. Neurosci. Res.* **85**, 2620–2630 (2007).
 57. Lopez, B. J. & Valentine, M. T. The +TIP coordinating protein EB1 is highly dynamic and diffusive on microtubules, sensitive to GTP analog, ionic strength, and EB1 concentration. *Cytoskeleton* **73**, 23–34 (2016).
 58. McVicker, D. P., Hoepflich, G. J., Thompson, A. R. & Berger, C. L. Tau Dynamics on the Microtubule Surface Modulate Kinesin Motility in an Isoform and Lattice Specific Manner. *Biophys. J.* **104**, 323a–324a (2013).